ISSN 0915-633X

NATIONAL INSTITUTE FOR FUSION SCIENCE

Realization and Classification of Symmetric Stellarator Configurations through Plasma Boundary Modulations

M. Yokoyama, N. Nakajima and M. Okamoto

(Received - Sep. 29, 1997)

NIFS-522 Dec. 1997

RESEARCH REPORT
NIFS Series

NAGOYA, JAPAN

Realization and Classification of Symmetric Stellarator Configurations through Plasma Boundary Modulations

M.Yokoyama, N.Nakajima, M.Okamoto

National Institute for Fusion Science, Toki, 509-52, Japan

Abstract

The basic roles of several principle modulations of plasma boundary shape on magnetohydrodynamic (MHD) equilibria are investigated. The appropriate combination of principle helical modulations for elimination of bumpy field component to realize the quasi-axisymmetric (QAS) and quasi-helically symmetric (QHS) configurations is explained by considering the variation of area of magnetic surface cross sections. The triangular modulation is effectively utilized to form the magnetic well by shifting the magnetic axis outward compared to the center of mass of magnetic surface cross section. The spatialization of the magnetic axis or the bumpy modulations of plasma boundary is rather important to reduce the toroidicity in the magnetic field, which can lead to QHS configurations. Some stellarator magnetic configurations under design activity or in the existing experimental device are mentioned from the point of views of plasma boundary modulations. Based on these principle understandings of plasma boundary modulations, examples of essential approach to QAS and QHS configurations are demonstrated step by step. The possibility of quasi-bumpy (or poloidally) symmetric (QBS) configuration is also mentioned.

KEYWORDS

plasma boundary modulations, magnetic field spectra, Boozer coordinates, symmetric stellarator configurations

1 Introduction

Stellarator magnetic configurations have a large flexibility to consider the improvement or optimization of plasma confinement properties due to their three dimensional properties.

In conventional stellarators, magnetic configuration studies have been done based on the intuitively determined coil configurations. The polarity of helical coils, combinations of helical, poloidal and toroidal coils, the minor radius and the pitch modulation of helical coil, the field period number etc, are the basic parameters of the coil system for changing the magnetic field properties. Usually, the determination for parameter space of the coil system corresponds to the designation of its topology. For example, the heliotron magnetic field, which has been successfully investigated in Kyoto University (the most recent experimental device is the Heliotron-E [1]) and develops for the Large Helical Device (LHD) [2] under construction at National Institute for Fusion Science (NIFS), is based on combinations of helical coils with polarity of $L = 2$ and poloidal coils. It is noted that the proposal for the next experimental device at Kyoto University is based on the modulated $L = 1$ helical coil system [3].

The magnetic configuration can be controlled by the plasma boundary modulations because MHD equilibria can be specified by boundary value problem with given pressure and current profiles [4]. Therefore, the magnetic configuration can be optimized to have desired physical criteria based on plasma boundary modulations [5]. J. Nührenberg explored the established method to construct the stellarator magnetic field without giving any specifications of the coils system. The quasi-helically symmetric (QHS) concept [6] is obtained by this approach. It realizes the helical symmetry in the Boozer coordinates [7] in a good approximation, although it is the torus geometry in the real coordinates. The Boozer coordinates are chosen to describe the magnetic field structure because the guiding center motion of charged particles are easily calculated by solving the guiding center equations [8]. Due to the presence of invariants of charged particle motions in the symmetric magnetic field, the plasma particles are confined in the finite volume, which gives better particle confinement properties compared to the non-symmetric magnetic field. Therefore, the flexible construction of magnetic field spectrum in the Boozer coordinates indicates the approach to the improvement of particle orbit confinement in stellarators. The QHS configuration is one example.

On the other hand, M. Y. Isaev et al., have considered the condition for quasi-symmetric configurations in a general invariant form independent of coordinates [9]. They discussed the possibility of several quasi-symmetric configurations which have different numbers of rotation of elliptic magnetic surface cross section with respect to the normal direction of the magnetic axis.

The experimental realization of such magnetic configurations involves the problem of finding a distribution of external coil currents which produces a magnetic field main-

taining the plasma equilibrium and satisfying the boundary conditions at the plasma boundary, $\boldsymbol{B}_v \cdot \boldsymbol{n} = 0$ and $\boldsymbol{B}_v^2 = \boldsymbol{B}_p^2 + 2P$, where $\boldsymbol{n}$ is the exterior normal vector to the boundary and P is the plasma pressure. Calculation of magnetic field in the vacuum region (outside the plasma) leads to a boundary value problem, which is not well posed for an elliptic partial differential equation for the magnetic potential. Moreover, the singularities often happen, which correspond to currents appearing too close to the plasma boundary. These difficulties may be resolved if one does have an interest in an approximate solution of the boundary value problem as shown by Merkel [10]. The external vacuum field can be represented by superposing harmonic functions such as Dommaschk potentials [11] for such a solution. This solution yields a vacuum field which is regular in the whole domain bounded by the chosen outer surface. This vacuum field uniquely determined by the plasma boundary shape can be used to find the position of the coils. The current lines on the outer surface may be shaped in such a way that closed current lines are discretized into a finite number of (modular) coils. Such modular coil configurations are designed for the Wendelstein 7-X (W7-X) [12] and the HSX [13].

Several concepts to improve the plasma confinement properties in stellarators have been proposed based on this approach. In QHS configurations, the essential point for improvement of reflected particle confinement is to eliminate the toroidal effects and to restore helical symmetry for magnetic field in the Boozer coordinates. It is noted that the HSX corresponds to the torus geometry with the aspect ratio 240 from the viewpoint of the magnetic field [13], although its real geometrical aspect ratio is about 8. However, the bootstrap current is expected to flow even in the QHS configurations [14] in the opposite direction to that in tokamaks. It is particularly dangerous in low shear stellarators such as the HSX, in which the rotational transform has to be carefully adjusted to avoid low order rational surfaces. For the reduction of bootstrap current to keep the good quality of vacuum magnetic surfaces even in finite beta plasmas, the appropriate combination of helical, toroidal and bumpy field components can be utilized [15]. This appropriate combination of magnetic field spectra is employed in the W7-X, although the helically symmetric property is not maintained.

Another concept of symmetric stellarator magnetic field is the quasi-axisymmetric (QAS) configuration [16, 17]. In QAS configurations, the helical magnetic field is reduced to be negligibly small and magnetic field structure in the Boozer coordinates is rather similar to that in tokamaks. Therefore, QAS configurations can also be considered as the tokamak configurations without the necessity of plasma current for MHD

equilibria. Their MHD properties and the effects of bootstrap current on MHD equilibria have been studied [18] to improve this concept further.

The magnetic surface cross sections (or plasma boundary shape) are different each other among QAS, QHS and W7-X, for example, indentation, triangularity and magnetic axis excursion etc, based on different desired physical criteria. These magnetic configurations are usually obtained by using the linear programming approach with numerous calculations for plasma boundary shaping. However, approaches to these configurations are not so well known, because usually only the finally obtained magnetic configurations are described to study its plasma confinement properties. It is important to grasp the approach itself or the basic roles of plasma boundary modulations to consider more favorable stellarator magnetic configurations. Therefore, approaches to some symmetric stellarator configurations are emphasized in this paper rather than their plasma confinement properties. Only the vacuum cases are considered here and finite beta effects are not taken into account. The appropriate coil configurations are also beyond the scope of this paper.

This paper is organized as follows. In Section 2, basic roles of several plasma boundary modulations on MHD equilibria are described. Section 3 will be devoted to demonstrate the essential approaches to QAS and QHS configurations based on several modulations described in Section 2. The concept of quasi-bumpy (or poloidally) symmetric (QBS) configuration is also proposed as an application of this study, although the detailed study for its plasma confinement properties will appear in a separate paper. Finally, summary and some discussions will be mentioned in Section 4.

2 Magnetic Configuration Control with Plasma Boundary Modulations

In order to clarify the basic roles of plasma boundary modulations, several effects of them on MHD equilibria have been studied by the fixed boundary version of three dimensional equilibrium code, VMEC [19]. The plasma boundary can be Fourier decomposed in the cylindrical coordinates (R, ϕ, Z) as

$$\begin{aligned} R(s,\theta_V,\zeta_V) &= \sum_{mn} R_{mn}(s)\cos(m\theta_V - nM\zeta_V), \\ Z(s,\theta_V,\zeta_V) &= \sum_{mn} Z_{mn}(s)\sin(m\theta_V - nM\zeta_V), \end{aligned} \tag{1}$$

where s is the magnetic surface label and θ_V (ζ_V) is the poloidal (toroidal) angle and m (n) is the poloidal (toroidal) mode number in the VMEC coordinates. Here, M is the

field period number. The left handed coordinate system for boundary Fourier modes are employed in this paper.

We choose the exact axisymmetric configuration described by $R_{00} = 2.0$ m, $R_{10} = 0.4$ m, $Z_{00} = 0.0$ m and $Z_{10} = 0.6$ m as the basic configuration for this study. This choice of principle elongation, $Z_{10}/R_{10} = 1.5$, is just for reference, and it is close to that for the reference QAS configuration in ref. [18]. The effective toroidicity of magnetic field becomes smaller if Z_{10}/R_{10} is increased because the average plasma radius becomes larger with keeping the width of magnetic surface cross sections in the major radius direction. The magnetic surface cross sections at three different poloidal cross sections, at $\phi = 0, (1/4)(2\pi/M)$ and $(1/2)(2\pi/M)$ for this configuration are shown in Fig. 1, where only one cross section can be seen due to its pure axisymmetry.

This configuration corresponds to tokamak configurations without plasma current, and therefore, the rotational transform ι is exactly zero. The ratio of the magnetic axis (R_{axis}) to the center of mass of magnetic surface cross section in the major radius direction ($R_{C.M.}$) at four poloidal cross sections with the interval of 1/4 toroidal period is also considered for the measurement of vacuum magnetic well. The average ratio of $R_{axis}/R_{C.M.}$ is greater than 1, which implies that the magnetic axis is shifted outward compared to the center of mass of magnetic surface cross section. In this configuration, the vacuum magnetic well is evaluated to be about 5%. Here, the magnetic well is defined by $(V'(0) - V'(\psi_T))/V'(0)$, where V is the volume enclosed by the magnetic surface corresponding to the toroidal flux function ψ_T and the prime denotes the derivative with respect to ψ_T.

In the following, the basic roles of boundary Fourier harmonics on MHD equilibria are described. It is noted that MHD equilibrium properties can also be varied due to change of geometrical aspect ratio and the field period number. In other words, MHD equilibrium properties are different in the configurations with the same plasma cross sections with different geometrical aspect ratio and/or field period number. Therefore, before proceeding into discussions of plasma boundary shaping, effects of geometrical aspect ratio A_p and field period number M are investigated.

2.1 Geometrical Aspect Ratio: A_p

First of all, effects of geometrical aspect ratio, A_p, on MHD equilibria are described with using the basic configuration as an example. Figure 2 (a) shows the magnetic surface cross sections for four configurations with different A_p with keeping the shape of magnetic surface cross sections. It is noted that the surfaces colored blue corresponds

to the basic configuration. The normalized magnetic field strength on the euqatorial line (in the Boozer coordinates) is shown with the corresponding colors in Fig. 2(b) for four axisymmetric configurations shown in Fig. 2(a). It is easily seen that the variation of field strength becomes smaller as the major radius is increased. The toroidicity in the magnetic field has $1/R$ dependence as well known, and therefore, the magnetic configuration with smaller A_p feel its toroidicity stronger than that for configurations with larger A_p. The ratio of toroidicity in the Boozer coordinates (B_{10}) to the geometrical inverse aspect ratio (a/R_{maj}), $B_{10}/(a/R_{maj})$, is 0.91 ($R_{maj} \sim 1$ m), 0.90 ($R_{maj} \sim 2$ m), 0.86 ($R_{maj} \sim 4$ m), 0.83 ($R_{maj} \sim 8$ m), respectively. Here R_{maj} denotes the major radius of magnetic axis and a the average plasma minor radius. Therefore, increasing A_p with keeping the magnetic surface cross sections is favorable to reduce the toroidicity in the magnetic field. This tendency can be utilized to obtain QHS and QBS configurations. This variation of effective toroidicity in the magnetic field is the essential role of A_p variation.

2.2 Field Period Number: M

In this subsection, roles of field period number, M, are described. The basic configuration is pure axisymmetric one, and therefore, effects of field period number can not be investigated. Thus, we consider the magnetic configuration with the elliptic magnetic surfaces described with boundary Fourier harmonics as: $R_{00} = 5.0$ m, $R_{10} = 1.0$ m, $Z_{10} = 1.5$ m, $R_{11} = -0.5$ m and $Z_{11} = 0.75$ m. The three different field period numbers, $M = 2, 5$ and 10, are compared here. The magnetic surface cross sections are shown in Fig. 3.1(a) for configurations with $M = 2$, Fig. 3.2(a) for $M = 5$ and Fig. 3.3(a) for $M = 10$. The magnetic surface cross section at $\phi = 0$ ($(1/4)(2\pi/M)$, $(1/2)(2\pi/M)$) is colored green (blue, red), respectively. The outermost magnetic surface cross section is exactly the same in these configurations due to the same Fourier components, however: inner magnetic surfaces are different each other. Therefore, MHD equilibria are expected to be different depending on M.

The magnetic field structure is considered in the Boozer coordinates [7], where the magnetic field strength B is expressed as

$$B = \sum_{mn} B_{mn}(r) \cos(m\theta_B - nM\zeta_B). \tag{2}$$

Here θ_B (ζ_B) is the poloidal (toroidal) angle in the Boozer coordinates, r denotes the average radius and m (n) the poloidal (toroidal) mode number. It is noted that B_{00} line (colored black) denotes the difference of B_{00} between at r and at the magnetic axis,

$B_{00}(r) - B_{00}(0)$, and all other components are normalized with $B_{00}(0)$. The magnetic field spectra in the Boozer coordinates are shown in Fig. 3.1(b) for configurations with $M = 2$, Fig. 3.2(b) for $M = 5$ and Fig. 3.3(b) for $M = 10$. The B_{00} component approximately measures the vacuum magnetic well/hill, and represents that the vacuum magnetic hill is strongly enhanced as M is increased. It is also easily seen that the B_{11} component is suppressed and, on the other hand, B_{21} component is enhanced as M is increased. This tendency can be understood by the following considerations. The magnetic surface cross sections shown in Figs. 3 are similar to those obtained by $L = 2$ helical coils such as the LHD or the Heliotron-E. Therefore, let us imagine that these configurations are formed with $L = 2$ continuous helical coils. In that case, $L = 2$ helical coils wind much looser in lower M cases because the toroidal period length is longer due to the fixed major radius. In other words, $L = 2$ helical coils in lower M cases behave as poloidal coils, and therefore, it causes only small deviation from axisymmetric magnetic field. On the other hand, they become "real" $L = 2$ helical coils as M is increased or the toroidal period length becomes shorter and thus the magnetic field component with the poloidal mode number (m) of 2 is strongly enhanced. The rotational transform for tightly wound $L = 2$ helical coils approximately depends on average radius r/a as [20]

$$\iota(r) \propto [1 + (M/R_{maj})^2 r^2/2] .$$

This dependence can be observed in Fig. 4, where ι per period for $M = 2, 5$ and 10 cases are shown. It is shown that the higher M gives stronger increase (shear) of ι toward the plasma boundary. The $\iota(0)$ reduces as M is increased, which arises from the relatively larger ratio of toroidal field to poloidal one due to tighter helical coil winding in larger M cases with the fixed major radius. It is noted that these dependences of vacuum magnetic well/hill and magnetic shear on M imply that the compatibility of these properties is rather difficult.

The above described variations of magnetic properties depending on M can also be observed for configurations such as a QAS configuration [18] by changing M. The remarkable difference is that the helical component with $m = 1$ is also strongly enhanced to become comparable to $m = 2$ component.

In the rest of this section, $M = 2$ cases are considered to investigate the roles of plasma boundary modulations. The above descriptions imply that MHD equilibria can be controlled by changing M even without modulating the plasma boundary shape. Therefore, it is noted that the following descriptions are well valid for $M = 2$ case, and should be carefully considered to apply to different M cases.

2.3 Principle Helical Modulations: $R_{11}, Z_{11}, R_{1,-1}$ and $Z_{1,-1}$

Among several plasma boundary modulations, principle helical modulations are firstly considered. These Fourier harmonics, especially R_{11} and Z_{11}, appear in several magnetic configurations including the planar axis configurations (such as the LHD [2] and the Heliotron-E [1]) or the spatial axis configurations (such as the W7-X [12] and QAS configurations [18]).

When we apply the modulation R_{11} with $R_{11}/R_{10} = -0.5$ on the basic configuration, the magnetic surface cross sections change as shown in Fig. 5(a).

The local rotational transform, $\hat{\iota}$, is also considered to grasp the behavior of magnetic field line winding quantitatively. It should be noted that the global and local rotational transform are denoted by its value per a field period in this paper. The understandings for magnetic field line winding will be helpful to control the global rotational transform, shear (increase or decrease) and to control the local magnetic curvature for ballooning mode stability [21, 22]. The $\hat{\iota}$ is calculated by using the contravariant components of magnetic field as

$$\hat{\iota} = \frac{d\theta_V}{d\zeta_V} = \frac{B^\theta}{B^\zeta} = \frac{\iota - \dfrac{\partial \lambda}{\partial \zeta}}{1 + \dfrac{\partial \lambda}{\partial \theta}} \tag{3}$$

from the description of magnetic field in the VMEC,

$$\boldsymbol{B} = \nabla\zeta_V \times \nabla\psi_T + \nabla\psi_P \times \nabla\theta_V^* = B^\theta \boldsymbol{e}_\theta + B^\zeta \boldsymbol{e}_\zeta, \tag{4}$$

where $2\pi\psi_T(s)$ and $2\pi\psi_P(s)$ are the toroidal and poloidal magnetic fluxes enclosed by the magnetic surface labelled by s and

$$\theta_V^* = \theta_V + \lambda(s, \theta_V, \zeta_V) \tag{5}$$

is the poloidal angle that makes the magnetic field line straight [23]. The $\boldsymbol{e}_\theta$ and $\boldsymbol{e}_\zeta$ are the covariant basis vectors.

Figure 5(b) shows $\hat{\iota}$ profile on the outermost magnetic surface. It is defined that $\hat{\iota}$ is positive for increasing poloidal angle as toroidal angle is increased along the magnetic filed line. It can be seen that $\hat{\iota}$ is larger around $\phi \sim (1/2)(2\pi/M)$, where the magnetic surface is elongated horizontally and $\hat{\iota}$ is negative around $\phi \sim 0$, where the magnetic surface is elongated vertically. The ι is around 0.05. This $\hat{\iota}$ structure is almost the same even for inner magnetic surfaces, for example, for $r/a = 0.3, 0.6$, which implies that the plasma boundary modulation with R_{11} does not form the global magnetic shear in $M = 2$ case. It is noted that $R_{axis}/R_{C.M.}$ becomes less than 1 around $\phi \sim (1/2)(2\pi/M)$,

which also decreases the average value of $R_{axis}/R_{C.M}$ to around 1. The magnetic well becomes shallower compared to the basic configuration reflecting to this fact.

As for Z_{11} with $Z_{11}/R_{10} = 0.75$, the magnetic surface cross sections are shown in Fig. 6(a), where the magnetic surface cross section is vertically elongated significantly around $\phi \sim 0$. As in R_{11} case, $\hat{\iota}$ is positive and large around the toroidal angle where the magnetic surface cross section is vertically elongated as shown in Fig. 6(b). This modulation also does not give global magnetic shear. Therefore, it can be said that the principle helical modulations are effective to form finite ι, however; they do not give the global magnetic shear in $M = 2$ case. As shown in Fig. 5(a) and 6(a), magnetic surface cross sections obtained by principle helical modulations R_{11} and Z_{11} do not change as the average radius r/a is increased. This is the reason for little global magnetic shear for principle helical modulations in $M = 2$ case. Contrary to this, in $M = 10$ case as shown in Fig. 3.3(a), magnetic surface cross sections change as r/a is increased, which results in the formation of global magnetic shear. The ratio, $R_{axis}/R_{C.M.}$, is the maximum at the vertically elongated cross section, that is, at $\phi = 0$. The average value of $R_{axis}/R_{C.M.}$ is still greater than 1, although it is smaller than that in the basic configuration. The magnetic well depth is reduced to about 3.9% from about 5% in the basic configuration.

Figures 7 show the magnetic field spectra in the Boozer coordinates for (a)$R_{11}/R_{10} = -0.5$ and (b)$Z_{11}/R_{10} = 0.75$ cases, respectively. It is clearly seen that the bumpy or mirror component, B_{01}, is significantly enhanced due to the magnetic flux conservation, which enhances the magnetic field strength around the toroidal angle where the area of magnetic surface cross section becomes small. The area is the smallest at $\phi = 0$ for $R_{11}/R_{10} = -0.5$ case, on the other hand, it is the case at $\phi = (1/2)(2\pi/M)$ for $Z_{11}/R_{10} = 0.75$ case. Therefore, the sign of B_{01} is opposite each other in Figs. 7. Also, the amplitude of B_{01} can be estimated from the variation of area of magnetic surface cross sections along the toroidal direction when the magnetic axis excursion is not remarkable. For example, in $R_{11}/R_{10} = -0.5$ case, the area of magnetic surface cross section at $\phi = (1/2)(2\pi/M)$ is characterized by $(R_{10} - R_{11}) \times Z_{10}$ and that at $\phi = 0$ by $(R_{10} + R_{11}) \times Z_{10}$. The ratio of area variation to the total area of magnetic surface cross sections at $\phi = 0$ and at $\phi = (1/2)(2\pi/M)$, that is, $|\{(R_{10} - R_{11}) - (R_{10} + R_{11})\}/\{(R_{10} - R_{11}) + (R_{10} + R_{11})\}| = 1/2$, and therefore, the bumpy field component B_{01} is around 50%.

This consideration can be applied to eliminate B_{01} with non-zero ι. Here one example is shown to demonstrate this statement clearly. As described above, helical

modulation with $R_{11}/R_{10} = -0.5$ and $Z_{11}/R_{10} = 0.75$ create the opposite bumpy component with almost the same absolute amplitude. Therefore, when we apply these two helical modulations simultaneously on the basic configuration as shown in Fig. 8(a), B_{01} is significantly suppressed as in Fig. 8(b). This combination makes the area of magnetic surface cross sections at $\phi = 0$ and $\phi = (1/2)(2\pi/M)$ almost the same. This will be explained later again more quantitatively. The average value of $R_{axis}/R_{C.M.}$ is below 1 reflecting to the fact that $R_{11}/R_{10} = -0.5$ and $Z_{11}/R_{10} = 0.75$ both reduce this average value from that in the basic configuration. The magnetic well is converted to magnetic hill of about 2.6%. It is noted that ι is about 0.18. This value of ι is not the simple summation of ι for $R_{11}/R_{10} = -0.5$ and $Z_{11}/R_{10} = 0.75$ cases because the combination of two Fourier boundary harmonics causes modulations with different mode numbers through the change of basis poloidal angles for Fourier representation. However; it is valuable to grasp the principle roles of basic plasma boundary modulations on MHD equilibria for considering how to obtain the magnetic configurations with desired properties.

In many magnetic configurations considered in present and future helical devices, R_{11} and Z_{11} are relatively larger compared to other boundary Fourier harmonics. The frequently observed variation of magnetic surface cross sections is vertically elongated shape around $\phi \sim 0$, the inclined one around $\phi \sim (1/4)(2\pi/M)$ and horizontally elongated one around $\phi \sim (1/2)(2\pi/M)$. This behavior is determined to large extent by the combinations of R_{11} and Z_{11} as shown in Fig. 8(a). Of course, several other boundary harmonics play important roles on MHD equilibria, however; the most dominant boundary harmonics are usually R_{11} and Z_{11}. Therefore, wide range of (R_{11}, Z_{11}) has been studied to grasp the general dependence of MHD global equilibrium properties on combinations of R_{11} and Z_{11} applied on the basic configuration. Figures 9 show (a) $\iota(0)$, (b) vacuum magnetic well (%) (negative value for vacuum magnetic hill) and (c) $B_{01}(0)$, respectively as a function of (R_{11}, Z_{11}). It is seen that the general tendency that $\iota(0)$ increases and magnetic well depth reduces as R_{11} and Z_{11} are increased with the opposite sign each other. It is noted that B_{01} is significantly enhanced when R_{11} and Z_{11} have the same sign, which is easily expected from the above descriptions for roles of R_{11} and Z_{11}. It may imply the possibility of a QBS configuration, and an example will be described in Section 3.

The magnetic surface cross sections become narrower if the plasma boundary is modulated only with R_{11} and Z_{11} to obtain higher ι with keeping B_{01} small as seen from Figs. 9(a) and 9(c). However, too narrow magnetic surface cross sections may

not be appropriate for experiments, for example, when the impurities and neutrals from the plasma facing components are considered. The helical modulations $R_{1,-1}$ and $Z_{1,-1}$, which have a different phase for toroidal angle to that of R_{11} and Z_{11}, are effective to avoid too narrow magnetic surface cross sections compatible with finite ϵ and small B_{01}.

As described above, the variation of area of magnetic surface cross sections along the toroidal direction greatly governs the amplitude of bumpy field component as long as the magnetic axis excursion is not remarkable. Therefore, it is important to make the area of magnetic surface cross section at $\phi = 0$ and $\phi = (1/2)(2\pi/M)$ almost the same to eliminate B_{01}, for example, when QAS and QHS configurations are desired. Here, the appropriate combinations of R_{11}, Z_{11}, $R_{1,-1}$ and $Z_{1,-1}$ are explained to eliminate B_{01}.

The half width (half height) of magnetic surface cross section at $\phi = 0$ is denoted by $R_{10}+R_{11}+R_{1,-1}$ $(Z_{10}+Z_{11}+Z_{1,-1})$ and the area is characterized by their product. On the other hand, the area at $\phi = (1/2)(2\pi/M)$ is characterized by $(R_{10} - R_{11} - R_{1,-1}) \times (Z_{10} - Z_{11} - Z_{1,-1})$. The condition that the area of magnetic surface cross sections at $\phi = 0$ and at $\phi = (1/2)(2\pi/M)$ are almost the same leads to the relation,

$$E_{RZ} \times (R_{11} + R_{1,-1}) \sim -(Z_{11} + Z_{1,-1}), \tag{6}$$

where E_{RZ} is the parameter to represent the principle ellipticity of magnetic surface cross section defined by Z_{10}/R_{10}. The magnetic configuration shown in Fig. 8(a) with $R_{11} = -0.2$ m, $Z_{11} = 0.3$ m and $E_{RZ} = 1.5$ almost satisfies eq. (6). It should be mentioned in Fig. 9(c) that the line connecting between $(R_{11}/R_{10}, Z_{11}/R_{10}) = (-0.6, 0.9)$ and $(0.6, -0.9)$ to eliminate B_{01} corresponds to eq. (6).

First, the basic properties of $R_{1,-1}$ and $Z_{1,-1}$ are explained. When the modulation with $R_{1,-1}/R_{1,0} = 0.1$ is applied on the basic configuration, the magnetic surface cross section is inclined as in negative R_{11} or positive Z_{11} case, although the magnetic surface cross section at $\phi = 0$ has a tendency to be horizontally elongated. This cross section is narrow in $R_{11}/R_{10} = -0.5$ case, and therefore, this $R_{1,-1}$ is effective to avoid the appearance of too narrow magnetic surface cross section around $\phi \sim 0$. In this case, vertically elongated cross section appears around $\phi \sim (1/2)(2\pi/M)$, and $R_{axis}/R_{C.M.}$ is the largest there. The average of $R_{axis}/R_{C.M.}$ is smaller than that in the basic configuration, however; it is still above 1, and the vacuum magnetic well still exists about 4.5%. As for $Z_{1,-1}/R_{10} = 0.1$ case, the significant feature is the behavior of magnetic axis position. All three cross sections are kept to be vertically elongated even at $\phi \sim (1/2)(2\pi/M)$. The $R_{axis}/R_{C.M.}$ becomes larger in the entire field period than

that in the basic configuration, and therefore, the average value is also well above 1, which indicates the deeper vacuum magnetic well (about 9.5%). The ι is rather small on the order of 10^{-2} for both $R_{1,-1}$ and $Z_{1,-1}$ cases because of their relatively small fractions to R_{10}. Both modulations have a tendency to arise relatively large negative B_{01} with relatively small modulation of plasma boundary (about $-25\%(-18\%)$ for $R_{1,-1}/R_{10} = 0.1(Z_{1,-1}/R_{10} = 0.1)$ case). Therefore, these modulations can be utilized instead of Z_{11} to avoid the appearance of too narrow magnetic surface cross sections compatible with finite ι, vacuum magnetic well and negligible B_{01} to realize QAS and QHS configurations.

Here three consecutive examples are shown to demonstrate above descriptions. The combinations of $R_{11}, Z_{11}, R_{1,-1}$ and $Z_{1,-1}$ are selected to satisfy eq. (6) as listed in Table I. Here "Conf. 1" denotes the magnetic configuration shown in Figs. 8.

The magnetic surface cross sections are shown in Figs. 10(a) for "Conf. 2" and (b) for "Conf. 3". It can be seen that the magnetic surface cross sections have a tendency to become less narrower especially around $\phi \sim 0$. The ι decreases due to the reduced Z_{11} in Confs. 2 and 3, however; $Z_{1.-1}$ effectively enhances the magnetic well as explained above. The B_{01} is effectively suppressed to small amplitude with these combinations, although the higher order bumpy field B_{02} appears. More precise considerations including not only the area of magnetic surface cross section at $\phi = 0$ and at $\phi = (1/2)(2\pi/M)$ but also that at $\phi = (1/4)(2\pi/M)$ are necessary to eliminate B_{02}.

Finally, the combinations of these four principle helical modulations in the W7-X are mentioned. The reference [24] lists the Fourier harmonics of representative three magnetic configurations in the W7-X, called "low-ι", "standard" and "high-ι" configurations. Table II summarizes the parameter E_{RZ}, ratios R_{11}/R_{10}, Z_{11}/R_{10}, $R_{1,-1}/R_{10}$ and $Z_{1,-1}/R_{10}$ and the residue of eq. (6), $E_{RZ} \times (R_{11} + R_{1,-1}) + (Z_{11} + Z_{1,-1})$, which is a measure of the difference of area of magnetic surface cross sections between at $\phi = 0$ and at $\phi = (1/2)(2\pi/M)$. As listed in Table II, the ratios R_{11}/R_{10} and Z_{11}/R_{10} increase with the opposite sign each other to obtain higher ι, and this can be understood by the above descriptions for roles of R_{11} and Z_{11}. The negative residue of eq. (6) implies that the area of magnetic surface cross section at $\phi = 0$ is smaller than that at $\phi = (1/2)(2\pi/M)$, which causes the positive B_{01}. The B_{01} is carefully chosen in the W7-X to maintain neoclassical diffusivity low level even in the case where there is no quasi-helical symmetry and also to reduce the bootstrap current significantly [15]. Therefore, the ratios $R_{1,-1}/R_{10}$ and $Z_{1,-1}/R_{10}$ are controlled to maintain this residue negative appropriately as R_{11}/R_{10} and Z_{11}/R_{10} are varied.

It is also noted that the residue of eq. (6) is about 10^{-6} in the standard configuration for the LHD with negligibly small B_{01}.

2.4 Triangular Modulations: R_{21} and Z_{21}

The boundary harmonics R_{21} and Z_{21} can cause the triangular modulations due to poloidal coupling with, for example, R_{10} and Z_{10}.

When $R_{21}/R_{10} = 0.25$ is applied on the basic configuration, magnetic surface cross sections are changed to triangular ones as shown in Fig. 11(a). Figure 11(b) shows $\hat{\iota}$ profile for $r/a = 0.3, 0.6$ and 1.0 from top to bottom, respectively. The deviation of magnetic surface cross sections from elliptic ones is enhanced along the line connecting sharp points on magnetic surface cross sections, which gives the different $\hat{\iota}$ structure on different magnetic surfaces. This radial variation of $\hat{\iota}$ structure causes the global magnetic shear. The magnetic field line winds rapidly in the poloidal direction (positive $\hat{\iota}$) along the line on the plasma boundary from the right tip at $\phi = 0$ to bottom tip at $\phi = (1/4)(2\pi/M)$ and to left tip at $\phi = (1/2)(2\pi/M)$. In the region with $\theta_V = \pi$ apart from this line, the magnetic field line winds the opposite way in the poloidal direction, however; the contributions from positive $\hat{\iota}$ is slightly larger and ι is about $\iota(0)/\iota(a) = 2.4 \times 10^{-3}/2.7 \times 10^{-2}$. The magnetic field spectra are shown in Fig. 11(c). The area of magnetic surface cross sections is almost the same between at $\phi = 0$ and at $\phi = (1/2)(2\pi/M)$, and therefore, B_{01} is negligibly small. The $R_{axis}/R_{C.M.}$ is significantly enhanced around $\phi \sim 0$, where the magnetic surface cross section is deformed to the outward pointing D-shape. The inward pointing D-shape cross section appears around $\phi \sim (1/2)(2\pi/M)$, and $R_{axis}/R_{C.M.}$ is below 1 there. However, the average of $R_{axis}/R_{C.M.}$ is still above 1, which gives the deep magnetic well about 6.3%. The triangular modulation Z_{21} has almost the same effects as in R_{21} case when $Z_{21}/R_{10} = 0.25$ is applied on the basic configuration. However, in this case, the outward pointing D-shape cross section appears around $\phi \sim (1/2)(2\pi/M)$.

Finally in this subsection, the magnetic configuration (named the "Conf. 4") with both $R_{21}/R_{10} = 0.25$ and $Z_{21}/R_{10} = 0.25$ simultaneously on the "Conf. 1" is mentioned to clarify roles of triangular modulations in several stellarator configurations. Figure 12 shows the magnetic surface cross sections for the "Conf. 4". The cross section is indented at $\phi = 0$ due to R_{21} and becomes outward pointing D-shape cross section around $\phi \sim (1/2)(2\pi/M)$ due to Z_{21}. This variation of magnetic surface cross sections is familiar in the W7-X, QAS and QHS configurations. It is noted that $\iota(0)/\iota(a) = 0.147/0.173$ in this configuration, which has a larger global magnetic shear compared

to "Conf. 1".

2.5 Principle Bumpy Modulations: R_{01} and Z_{01}

The stellarator/heliotron/torsatron configurations are frequently divided into two categories; planar magnetic axis configurations (such as the standard configuration in the LHD and the Heliotron-E) and helical (or spatial) magnetic axis configurations (such as the W7-X and the HSX). Recently, theoretical study has been done for spatial axis configurations in the LHD by unbalancing the helical coil currents [25]. It is reported there that the direction of bootstrap current is strongly affected with the spatialization of the magnetic axis, which affects the Mercier stability [26]. Therefore, it is important to grasp the effects of the spatial axis (or the bumpy modulations of plasma boundary) on plasma confinement properties for global understandings of helical systems. In this subsection, the main roles of bumpy modulations of plasma boundary on MHD equilibria are explained.

Figure 13(a) shows the magnetic surface cross sections when the bumpy modulation with $R_{01}/R_{10} = 0.5$ is applied on the basic configuration. The magnetic axis shifts more outward around $\phi \sim (1/2)(2\pi/M)$, and also the average of $R_{axis}/R_{C.M.}$ is greatly enhanced. This average value is significantly larger than that in the basic configuration and the magnetic well becomes deeper to about 8.5%. In the plasma boundary modulations described above, that is, principle helical modulations and triangular modulations, $R_{axis}/R_{C.M.}$ tends to have the minimum value around $\phi \sim (1/2)(2\pi/M)$, and this sometimes causes the magnetic hill or the shallow magnetic well. Therefore, the bumpy modulation with positive R_{01}/R_{10} is effective to avoid this matter for the formation of vacuum magnetic well. Figure 13(b) shows the magnetic field spectra in the Boozer coordinates. The notable point here is that the toroidicity B_{10} reduces from the geometrical inverse aspect ratio, a/R_{maj}, shown by the arrow. The ratio $B_{10}/(a/R_{maj})$ is about 0.89. This effect can be utilized to reduce B_{10}, for example, to realize QHS and QBS configurations as will be demonstrated in Section 3.

As for bumpy modulation in the vertical direction, when $Z_{01}/R_{10} = -0.5$ is applied on the basic configuration, the magnetic surface cross sections are changed as shown in Fig. 14(a). The only two cross sections are seen because the cross sections at $\phi = 0$ and at $\phi = (1/2)(2\pi/M)$ are the same. From the comparison between Fig. 14(a) and Fig. 1, the magnetic axis is not shifted more outward from $R_{C.M.}$, which gives the shallower magnetic well about 2.9%. The mod-B contours in $\phi = (1/4)(2\pi/M)$ do not coincide with $\theta_V = \pi/2$ and $\theta_V = 3\pi/2$ lines, and, this causes the relatively large

non-axisymmetric magnetic components B_{11} and $B_{1,-1}$ as shown in Fig. 14(b). In the case of $R_{01}/R_{10} = 0.5$, $B_{1,-1}$ appears with the opposite sign to this case as seen in Fig. 13(b), and therefore, the appropriate combination of R_{01} and Z_{01} has a possibility to cancel $B_{1,-1}$. It is noted that B_{10} is reduced to $B_{10}/(a/R_{maj}) = 0.89$ also in this case.

When both radial and vertical bumpy modulations R_{01} and Z_{01} are applied on the "Conf. 4" with $R_{01}/R_{10} = 0.5$ and $Z_{01}/R_{10} = -0.25$, the magnetic axis excursion becomes remarkable as shown in Fig. 15 compared to Fig. 12. The $\iota(0)/\iota(a) = 0.159/0.189$ in this configuration, which is a little bit larger than that in the "Conf. 4". The difference in ι from "Conf. 4", $\Delta\iota(0)/\Delta\iota(a) = 0.012/0.016$, arises from the bumpy modulations (or the spatialization of the magnetic axis) with $R_{01}/R_{10} = 0.5$ and $Z_{01}/R_{10} = -0.25$. This contribution is relatively small compared to that from R_{11} and Z_{11}. Therefore, it can be said that ι is determined by combinations of principle helical modulations R_{11} and Z_{11} to large extent.

It is noted that $B_{10}/(a/R_{maj})$ is reduced to 0.61 in this configuration. The decoupling of magnetic field structure from the real torus geometry is successfully realized with the spatialized magnetic axis. If much larger bumpy modulations of plasma boundary are considered, the magnetic configuration without B_{10} would be possible (such as QHS and QBS configurations). This will be explained in more detail in the approach to realize example QHS and QBS configurations in Section 3. Also, in ref. [27], the magnetic configurations with different ratios of B_{10}/B_{11} are investigated to study the collisionless alpha particle confinement, where the ratio B_{10}/B_{11} becomes smaller as the magnetic axis excursion is enhanced with keeping the magnetic surface cross sections roughly unchanged. This tendency is understandable from the above descriptions.

2.6 Several Other Modulations

The most dominant contributions of plasma boundary Fourier harmonics to plasma boundary shape usually arise from the above described modulations (for example, see ref. [24]). However; there are some other important modulations to control MHD equilibrium properties, although the amplitudes are not so large compared to the above described dominant harmonics. Here in this subsection, some of them are summarized for reference to make the statements in Section 3 more understandable.

Higher Order Axisymmetric Modulation: R_{20}

The higher order axisymmetric modulation R_{20} uniformly shifts the magnetic surfaces outward in the case of positive R_{20}/R_{10}. In the case close to axisymmetric mag-

netic field, the variation of magnetic field strength in the radial direction is smaller in the outerside of a torus as shown in Fig. 2(b). Therofore, the magnetic configurations shifted outward with the positive R_{20}/R_{10} feel less toroidicity in the magnetic field. The $B_{10}/(a/R_{maj})$ is reduced to 0.84 when $R_{20}/R_{10} = 0.125$ is applied on the basic configuration ($B_{10}/(a/R_{maj}) = 0.9$), although the higher order axisymmetric component B_{20} appears with a few percent.

Higher Order Helical Modulation: R_{22}

This modulation can also be considered as the triangular modulation twisted twice faster than R_{21} or Z_{21} in the toroidal direction. The area of magnetic surface cross sections at $\phi = 0$ and $\phi = (1/2)(2\pi/M)$ are the same and $R_{axis}/R_{C.M}$ is also the same at these two poloidal cross sections. In the case of positive R_{21}/R_{10}, $R_{axis}/R_{C.M}$ is the smallest at $\phi = (1/2)(2\pi/M)$ and it can cause the magnetic hill as described above. Therefore, positive R_{22}/R_{10} is effective to recover from this matter, which can form the magnetic well with relatively small modulation of plasma boundary shape.

The R_{22} also has the characteristic feature for twisting the magnetic field lines as in R_{21} and Z_{21} cases with the doubled periodicity in the toroidal direction. Therefore, the $\hat{\iota}$ has a similar structure (with doubled periodicity) as for triangular modulations. Figures 16 show the $\hat{\iota}$ structures at $r/a = 0.3, 0.6$ and 1.0 from top to bottom, respectively. It is seen that the global magnetic shear can be formed as in R_{21} case (cf., Fig. 11(b)). The ι is relatively large at the plasma boundary for relatively small modulation with $R_{22}/R_{10} = 0.125$ on the basic configuration ($\iota(a) \sim 1.6 \times 10^{-2}$) compared to that for $R_{21}/R_{10} = 0.25$ case ($\iota(a) \sim 2.3 \times 10^{-2}$).

It should be noted that this modulation has a tendency to cause B_{12}, for example, -5% for this case. This B_{12} should be eliminated for a purer magnetic field structure with, for example, the appropriate positive Z_{22}/R_{10} which causes the positive B_{12}.

3 Applications of Plasma Boundary Modulations to Realize Symmetric Stellarator Configurations

Several roles of plasma boundary modulations on MHD equilibria have been described in Section 2. In this section, those are applied to realize examples of QAS, QHS and QBS configurations. Usually, only the finally obtained magnetic configurations are explained in the papers, however; approaches to those configurations would also be valuable to understand to consider better or desirable magnetic configurations for

improvement of plasma confinement properties in helical systems.

Quasi-Axisymmetric Configuration

For obtaining QAS configurations, the main points are the elimination of the bumpy field component B_{01} and the main helical component B_{11}.

The initial configuration (QA1) (Fig. 17(a)) is chosen to have the combination of $R_{11}, Z_{11}, R_{1,-1}$ and $Z_{1,-1}$ which almost satisfies eq. (6). Several MHD equilibrium properties are summarized in Table Ⅲ. The three dominant non-axisymmetric magnetic field components to be suppressed are also listed for reference. The bumpy field components B_{01} and B_{02} usually have amplitudes even on the magnetic axis, and therefore, they are written such as $B_{01}(0)/B_{01}(a)$. All the other components are represented by their amplitude at the plasma boundary. The QA1 has a large B_{21} and B_{11}, and there is also a large B_{01} in the plasma core region, although it is rather small in the edge region due to the appropriate combination of principle helical modulations.

In the following, utilized boundary Fourier components are listed with their purposes to show an approach to a QAS configuration clearly.

R_{21}: reduction of B_{21} and B_{11} $\rightarrow$ successful, however; enhancement of vacuum magnetic hill (**QA2**),

Z_{21}: reduction of vacuum magnetic hill $\rightarrow$ successful, however; B_{21} increases a little again (**QA3**, Fig. 17(b)),

R_{20}: reduction of vacuum magnetic hill and B_{21} $\rightarrow$ large increase of $R_{axis}/R_{C.M.}$ in the entire field period, however; still vacuum magnetic hill (**QA4**, Fig. 17(c)),

R_{22} **and** Z_{22}: increase of $R_{axis}/R_{C.M.}$ to form vacuum magnetic well with keeping non-axisymmetric magnetic components small $\rightarrow$ successful (in the region of $r/a \lesssim 0.5$) (**QA5**, Fig. 17(d)),

R_{01}: enhancement of vacuum magnetic well $\rightarrow$ extension of vacuum magnetic well region (**QA6**),

$R_{2,-1}$: enhancement of vacuum magnetic well $\rightarrow$ vacuum magnetic well about 1% in the entire plasma region (**QA7**, Fig. 17(e)).

In the above approach, it is shown that the outward pointing triangular (or D-shape) cross section around $\phi \sim (1/2)(2\pi/M)$ and tear-drop shape cross section with $R_{axis}/R_{C.M.}$ greater than 1 around $\phi \sim (1/4)(2\pi/M)$ are very effective to reduce the

vacuum magnetic hill or to enhance the vacuum magnetic well. It is noted that these shaped cross sections typically appear in the W7-X, QAS and QHS configurations. The magnetic field spectra for the QA7 are shown in Fig. 17(f). It is noted that the line colored light blue corresponds to B_{20}, which is also the axisymmetric component. The B_{01} and B_{02} cut zero near the magnetic axis and their effects of symmetry breaking in the plasma core region are relatively well suppressed, although they have the amplitude of a few percent at the plasma boundary. The other dominant components have the poloidal mode number $m = 2$ and their contributions are also rather small in the plasma core region, where the plasma density is relatively higher compared to the plasma edge region. Therefore, it can be said that the QA7 is a QAS configuration. Of course, more careful controls of MHD equilibrium properties by large computations for plasma boundary modulations with more boundary Fourier harmonics would be necessary to obtain more sophisticated QAS configuration. However, the essential realization of a QAS configuration is possible based on the knowledge on the basic roles of important plasma boundary modulations. Especially, the suppression of bumpy field by considering the area of magnetic surface cross sections is essential factor. Also, the smaller M and/or smaller A_p is favorable to realize QAS configurations by considering the results shown in Section 2 due to its relatively weaker helical field contributions. It is noted that the QA7 has an aspect ratio about 2.7 with $M = 2$ [18].

It should be noted that the bumpy modulation is only applied with the small fraction $R_{01}/R_{10} \sim 0.12$ just to enhance $R_{axis}/R_{C.M.}$ around $\phi \sim (1/2)(2\pi/M)$ in the above approach to a QAS configuration. This role is also possible by other modulations, and therefore, the bumpy modulation or the spatialization of the magnetic axis is not the indispensable factor to realize QAS configurations.

Quasi-Helically Symmetric Configuration

In this subsection, an example of approach to a QHS configuration is explained. The point is to reduce the toroidicity in the magnetic field spectra or to decouple the magnetic configuration from the real torus geometry. Here, the field period number is chosen $M = 4$ for reference. It is noted that the HSX is also the device with $M = 4$. The extension to different M cases will be mentioned later.

The point to guess the initial configuration is to choose the combination of $R_{11}, Z_{11}, R_{1,-1}$ and $Z_{1,-1}$ with the appropriate elongation $E_{RZ} = Z_{10}/R_{10}$ to suppress B_{01}. This requirement is the same as in an approach to a QAS configuration.

Figure 18(a) shows the magnetic surface cross sections with the residue of about 6×10^{-3} in eq. (6) (named the QH1). Some MHD equilibrium properties are listed in

Table IV. The B_{01} is suppressed to some extent. It is noted that the toroidicity in the magnetic field (B_{10}) is comparable to the average geometrical inverse aspect ratio (a/R_{maj}) in the QH1.

The spatialization of the magnetic axis is effectively utilized to reduce B_{10}. The QH2 (Fig. 18(b)) is obtained with $R_{01}/R_{10} = -Z_{01}/R_{10} = 1.18$. The $B_{10}/(a/R_{maj})$ decreases to 0.18, although the vacuum magnetic hill becomes higher due to the role of positive Z_{01} as described in Section 2. Now, the largest magnetic field spectrum is B_{11}, which should be dominant in QHS configurations. Therefore, careful controls of plasma boundary shape to decrease the magnetic field spectra but B_{11} and to form the vacuum magnetic well should be pursued based on this configuration.

There are several possibilities of plasma boundary modulations for these purposes. Among them, triangular modulations with R_{21} and Z_{21} are considered here, because the dominant unfavorable magnetic spectrum B_{21} can be cancelled out with the negative contribution of B_{21} with the positive R_{21} as seen in Fig. 11(c) and Z_{21} is effective to form the vacuum magnetic well. The application of $R_{21}/R_{10} = Z_{21}/R_{10} \sim 0.26$ on the QH2 leads to the QH3 (Fig. 18(c)). The shallow magnetic well exists in this configuration with significantly small toroidicity, $B_{10} \sim -1.0\%$.

The considerations to obtain deeper vacuum magnetic well and to realize a purer structure of magnetic field have led to a configuration closer to QHS configuration. In this procedure, small fraction of $R_{20}/R_{10}, R_{22}/R_{10}$ etc, are utilized and the QH4 (Fig. 18(d)) is obtained. It is noted that the magnetic surface cross sections are indented around $\phi \sim 0$ and become more tear-drop shape around $\phi \sim (1/4)(2\pi/M)$ with these small modulations as compared to Fig. 18(c). The magnetic field spectra of the QH4 are shown in Fig. 18(e), where there are still some contributions from the magnetic spectra but B_{11}, and therefore, the large computations for plasma boundary modulations with more boundary Fourier harmonics would be necessary to obtain more sophisticated QHS configuration. However, the essential point to realize QHS configurations is the appropriate spatialization of the magnetic axis as explained above. It should be noted that the magnetic configuration designed for the HSX also has a large magnetic axis excursion [13], although the magnetic surface cross sections look different from those in the QH4.

Finally in this subsection, different M cases are mentioned. In the case of $M = 4$, the magnetic axis is spatialized with about $R_{01}/R_{10} = -Z_{01}/R_{10} \sim 1.2$ to reduce B_{10} significantly to the order of -1%. When the field period number of the QH4 ($M = 4$) is increased to $M = 5$ with keeping all the boundary Fourier harmonics unchanged,

B_{10} changes the sign from negative to positive with the amplitude of about 2%, and therefore, the spatialization of the magnetic axis can be reduced to eliminate B_{10}. The reduction of ratios, $R_{01}/R_{10} = -Z_{01}/R_{10}$, from about 1.2 to 0.66, and the small change of R_{20} (the increment of R_{20}/R_{10} is only about 0.03) to purify the magnetic field spectra lead to the configuration shown in Fig. 18(f) with $M = 5$, whose magnetic field spectra are shown in Fig. 18(g). This configuration is also close to a QHS configuration with the vacuum magnetic well about 1.4%.

As described above, there is a tendency that the larger magnetic axis excursion is necessary to reduce B_{10} for smaller M. This is easily seen in the Table V, where the applied ratios of $R_{01}/R_{10} = -Z_{01}/R_{10}$ are listed to reduce $|B_{10}|$ to the order of 1% in $M = 3, 4, 5$ and 6 systems with keeping all the other boundary harmonics almost unchanged from the QH4 with $M = 4$. It is noted that the configuration is rather far from QHS one in $M = 3$ and 6 cases, and also the magnetic well disappears in $M = 6$ case when only $R_{01}/R_{10} = -Z_{01}/R_{10}$ are changed from the QH4. Therefore, the listed ratio is just a reference to reduce B_{10} to relatively small amplitude in $M = 3$ and 6 cases. As expected from Table V, QHS configurations in $M = 2$ systems would not be practical because the significantly large magnetic axis excursion is required. This is understandable from subsection 2.2, where it is shown that the toroidicity in the magnetic field is relatively larger compared to helical fields in smaller M cases. Therefore, the larger magnetic axis excursion is required to suppress B_{10} in smaller M cases. It is also recognized that the configurations with larger aspect ratio are more suitable to realize QHS configurations due to its smaller toroidicity. It is noted that the QH4 has a geometrical aspect ratio about 11.5.

Quasi-Bumpy (Poloidally) Symmetric Configuration

Here, the possibility to realize a QBS configuration is mentioned based on basic roles of plasma boundary control, although the detailed discussions of confinement properties will appear in a separate paper.

In the above two subsections, the initial configurations are chosen to eliminate B_{01}, because it is the symmetry breaking component for QAS and QHS configurations. For QBS configurations, the toroidicity B_{10} is one of the components that should be eliminated, and therefore, the above obtained QHS configuration, QH4 with $M = 4$, is chosen for the initial configuration.

The principle helical modulation with the negative R_{11}/R_{10} plays a role to enhance the positive B_{01} as shown in Fig. 7(a). Therefore, when the sign of R_{11}/R_{10} is changed to positive, B_{01} is expected to have a negative sign. Of course, the B_{01} has a tendency

to have the positive sign when the sign of Z_{11}/R_{10} is reversed. Here, in this subsection, the former case is mentioned.

The ratio R_{11}/R_{10} is changed from about -0.1 to 0 starting from the QH4, the magnetic surface cross sections are deformed as shown in Fig. 19(a). This change of principle helical modulation (or breaking of eq. (6)) is the essential point to approach a QBS configuration. The area of magnetic surface cross section at $\phi = 0$ is significantly larger than that at $\phi = (1/2)(2\pi/M)$, which causes the large negative B_{01} on the order of -50%. In this configuration, B_{11} still has an amplitude about -12% and the magnetic hill about 1%, although $|B_{10}|$ is less than 0.6%.

The small changes of modulations such as triangular modulations (R_{21} and Z_{21}), higher order helical modulations (R_{22} and Z_{22}) etc, are utilized to reduce B_{11} and to form the vacuum magnetic well. These considerations have led to the magnetic configuration whose magnetic surface cross sections are shown in Fig. 19(b) and the magnetic field spectra in the Boozer coordinates in Fig. 19(c). The $\iota(0)/\iota(a)$ is 0.149/0.189 and the magnetic well exists about 1.8% in the entire plasma region.

This magnetic configuration can be considered as the linked mirror or the endless mirror configuration with the finite ι and vacuum magnetic well from the point of views of magnetic field structure in the Boozer coordinates. Because of finite ι, it is distinguishable from the so-called bumpy torus. The magnetic field strength varies in the poloidal direction very weakly (only through the remaining B_{11}). The bootstrap current is expected to be significantly small in a QBS configuration, which is an advantage to suppress finite beta effects rather small. However, in this example of a QBS configuration, B_{01} is significantly large and is almost comparable to the uniform magnetic field, which causes the large fraction of reflected particles to loss from the confinement region via drift motion due to B_{11}. Therefore, the reduction of B_{01} should be pursued with keeping the non-bumpy magnetic field components relatively small to obtain a QBS configuration with smaller fraction of reflected particles.

4 Summary and Discussions

The effects of plasma boundary modulations on MHD equilibria have been described, which are useful to realize desired stellarator magnetic configurations.

The principle helical modulations, which dominantly appear on many stellarator configurations, give the variation of area of magnetic surface cross sections between at the beginning of the field period ($\phi = 0$) and at the middle of the field period

($\phi = (1/2)(2\pi/M)$). Here M is the field period number. This variation causes the relatively large bumpy field component (B_{01}) due to the magnetic flux conservation, which is not suitable to realize quasi-axisymmetric (QAS) or quasi-helically symmetric (QHS) configurations. The appropriate combination of principle helical modulations to suppress B_{01} is presented, eq. (6), by considering the area of magnetic surface cross sections. The approach to avoid the appearance of too narrow magnetic surface cross sections is also mentioned and the consecutive magnetic configurations are demonstrated with keeping B_{01} relatively small.

The triangular modulations (especially in the vertical direction) can be utilized to form or deepen the vacuum magnetic well by shifting the magnetic axis outward compared to the center of mass of magnetic surface cross section. The favorable radial triangular modulation gives the indentation on the magnetic surface cross section around $\phi \sim 0$ and the favorable vertical one leads to the outward pointing triangular (or D-shape) cross section around $\phi \sim (1/2)(2\pi/M)$, which are frequently seen in the W7-X, QAS and QHS configurations. The possibility of global magnetic shear control by the triangular modulations is also shown.

The spatialization of the magnetic axis or the bumpy modulations of plasma boundary shape is also investigated. This is the significant feature to separate the helical systems into two categories, planar axis configurations (such as the standard configuration in the LHD and the Heliotron-E) and spatial axis configurations (such as the W7-X and the HSX). The significant feature of bumpy modulations is that the toroidicity in the magnetic field (B_{10}) is effectively reduced as the magnetic axis excursion is enhanced. In other words, the magnetic configuration is effectively decoupled from its real torus geometry. This is utilized in the HSX to realize a QHS configuration and also in the W7-X to reduce B_{10} to about half of geometrical inverse aspect ratio. The necessary magnetic axis excursion depends on M: the larger excursion is required as M is decreased because B_{10} becomes relatively larger compared to helical fields. Therefore, a QHS configuration in the system with smaller M, for example 2, would be rather difficult to realize.

Usually, the finally obtained magnetic configurations are shown in the papers to study their plasma confinement properties. However; approaches to them would also be rather valuable to grasp to consider more attractive or innovative stellarator magnetic configurations for further improvement or optimization of helical systems. Therefore, based on the knowledge on effects of plasma boundary modulations, realization of example QAS and QHS configurations are demonstrated step by step. The initial con-

figuration is chosen with the appropriate combination of principle helical modulations which satisfies eq. (6) for both cases.

The essential point to realize a QAS configuration is that the fine suppression of B_{01} by considering the area of magnetic surface cross sections. For the formation of vacuum magnetic well, efforts are made to realize the outward pointing triangular (or D-shape) cross section around $\phi \sim (1/2)(2\pi/M)$ and tear-drop shaped cross section around $\phi \sim (1/4)(2\pi/M)$. The bumpy modulation is just applied for this purpose, which can be replaced with the other modulation. Therefore, it can be said that the bumpy modulation or the spatilization of the magnetic axis is not the essential factor to realize QAS configurations. It is also intuitively recognized that the configurations with smaller M and/or with smaller aspect ratio A_p are suitable to realize QAS configurations due to the relatively larger toroidicity.

On the other hand, the reduction of B_{10} is indispensable factor to realize QHS configurations. This role is effectively played by the bumpy modulations of plasma boundary shape or the spatialization of the magnetic axis. The large magnetic axis excursion (about 10% of major radius) is applied to reduce the toroidicity in the magnetic field to about 1% in $M = 4$ systems. The requirements to form the vacuum magnetic well and to realize a pure magnetic field structure lead to the appropriate combination of triangular modulations. This application causes the indented cross section around $\phi \sim 0$ and the outward pointing triangular cross section around $\phi \sim (1/2)(2\pi/M)$. A QHS configuration in $M = 5$ system is also demonstrated by just reducing the bumpy modulations of plasma boundary shape. The relatively larger helical field contributions in larger M cases with the fixed major radius allow to reduce the magnetic axis excursion to suppress B_{10}. The configurations with larger A_p are also suitable to realize QHS configurations due to the relatively smaller toroidicity.

The possibility of a quasi-bumpy (or poloidally) symmetric (QBS) configuration is also mentioned. The breaking of eq. (6) gives the large B_{01} with either sign depending on the variation of area of magnetic surface cross sections. By utilizing this, the magnetic field with B_{01} dominantly is possible. This configuration has a finite ι, and therefore, it is distinguishable from the so-called bumpy torus. The bumpy field is too large in an example configuration (cf., Fig. 19(b)), which causes the large fraction of reflected particles. Therefore, the further detailed study is required to make the QBS concept more attractive, however; the third symmetric stellarator configuration, following QAS and QHS, would bring great interests also for connection between helical systems and mirror systems, because a QBS configuration can also be considered as a linked-mirror

(or endless mirror) configuration.

The above statements are summarized in Fig. 20, where classifications of QAS, QHS and QBS configurations are clearly shown. The key factors are B_{01} control via eq. (6), field period number (M), geometrical aspect ratio (A_p) and the magnetic axis excursion. It is noted that the scales of axes are different between QAS and (QHS, QBS) configurations, which explicitly indicates the difference of A_p between these configurations.

Here the heliac equilibria are mentioned for comparison to the above mentioned stellarator configurations such as the LHD, W7-X, QAS and QHS configurations because heliacs have a significantly different variation of plasma boundary shape. It has the bean-shaped cross section in the entire field period, which rotates along the toroidal direction with a relatively large magnetic axis excursion. The heliac equilibria are constructed mainly from the bumpy modulations, triangular modulations and helical modulations twisted twice faster than the principle helical ones (that is, R_{12} and Z_{12} rather than R_{11} and Z_{11}) of plasma boundary shape as seen in the VMEC input data for the H-1 heliac [28]. The principle helical modulations, which cause the inclined magnetic surface cross section around $\phi \sim (1/4)(2\pi/M)$, are rather small on the order of $R_{11}/R_{10} \sim 10^{-2}$. The R_{12} and Z_{12} play roles as the principle helical modulations play: for example, the appearance of bumpy field components due to the variation of area of magnetic surface cross sections and the formation of net rotational transform. The differences compared to principle helical ones are that the main bumpy field is B_{02} rather than B_{01} and ι is almost doubled. For example, $R_{12}/R_{10} = -0.5$ causes the $B_{02} \sim +50\%$ and ι is around 0.1 per a field period when it is applied on the basic configuration (cf., $B_{01} \sim +50\%$ and ι is around 0.05 for $R_{11}/R_{10} = -0.5$ case). This is the main reason for a higher ι in heliacs than that in the above mentioned configurations. For example, ι is around 0.4 per a period in the H-1 heliac [29] and, on the other hand, around 0.2 per a period in the W7-X [24]. Therefore, this helical modulation twisting faster would be useful to increase ι, for example, to reduce the Pfirsch-Schlüter current to obtain a higher equilibrium beta value [18].

In this study, Fourier representation of plasma bounday shape in the cylindrical coordinates are employed as in eq. (1). However; the distribution of poloidal angle θ_V is different in the cases, for example, in the basic configuration and the configuration with $R_{11}/R_{10} = -0.5$ applied on the basic configuration as easily seen in Fig. 1 and Fig. 5(a). In Fig. 1, the curve of $\theta_V = \pi/2$ is almost vertical, however; it is inclined around $\phi \sim (1/4)(2\pi/M)$ in Fig. 5(a). Because of this, the amplitude of Fourier boundary

harmonics depend on how many Fourier modes are used and what kind of angle variables are considered to represent the plasma boundary shape. In this sense, the absolute value of boundary Fourier amplitudes in this paper would not be so meaningful. However, the main object of this paper is to grasp basic roles of plasma boundary modulations and, as an application, to demonstrate approaches to realize some symmetric stellarator magnetic configurations based on these knowledge. Therefore, the approximate grasp connecting plasma boundary modulations with magnetic field structure in the Boozer coordinates is significantly useful.

The plasma confinement properties such as MHD stability and neoclassical transport are beyond the scope and are not mentioned in this paper. Only the formation of vacuum magnetic well is emphasized just to stabilize Mercier modes. However, some confinement properties in QAS and QHS configurations are already studied, for example, in ref. [13, 18]. The detailed confinement properties of QBS is now being studied and they will appear in a separate paper.

Recently, Nakajima has investigated that the relations between the high-mode-number ballooning stability and the local magnetic shear in heliotron/torsatron configurations with a large Shafranov shift [21, 22]. It is reported there that the ballooning mode eigenvalues have a strong dependence on the field line through the strong dependence on local magnetic curvature. The local magnetic curvature itself is determined or varied from MHD equilibrium properties, and therefore, the "external" control of local magnetic curvature by modulating the plasma boundary shape would affect the ballooning mode stability. This may explore the approach to stellarator magnetic configurations with ballooning stability up to high beta values. The applications of plasma boundary modulations to this problem is the subject of the future study.

Acknowledgements

The authors gratefully acknowledge productive and fruitful discussions with Prof. J. Nührenberg and Prof. M. Wakatani. Dr. C. Nührenberg is also appreciated to allow them to mention the W7-X boundary data listed in ref. [24]. They also acknowledge Dr. R. L. Dewar for allowing them to mention the H-1 heliac equilibrium.

References

[1] UO. K., et al., in Plasma Physics and Controlled Nuclear Fusion Research 1980 (Proc. 8th Int. Conf. Brussels, 1980), Vol.1, IAEA, Vienna (1981)217.

[2] IIYOSHI. A., et al., Fusion Technol. **17**(1990)169.

[3] YOKOYAMA, M., NAKAMURA. Y., WAKATANI. M. et al., in Plasma Physics and Controlled Nuclear Fusion Research 1996 (Proc. 16th Int. Conf. Montreal, 1996) to appear.

[4] HIRSHMAN, S. P., LEE, D. K., Comput. Phys. Commun. **39**(1986)161.

[5] NÜHRENBERG, J., ZILLE, R., Phys. Lett. **A114**(1986)129.

[6] NÜHRENBERG, J., ZILLE, R., Phys. Lett. **A129**(1988)113.

[7] BOOZER, A. H., Phys. Fluids **23**(1980)904.

[8] FOWLER, R. H., et al., Phys. Fluids **28**(1985)338.

[9] ISAEV, M. YU., MIKHAILOV, M. I., SHAFRANOV, V. D., Plasma Phys. Reports **20**(1994)357.

[10] MERKEL, P., Nucl. Fusion **27**(1987)867.

[11] DOMMASCHK, W., Comput. Phys. Commun. **40**(1986)203.

[12] GRIEGER, G., et al., Phys. Fluids **B4**(1992)2081.

[13] ANDERSON, D. T., et al., HSX — A Helically Symmetric Toroidal Experiment — (edited by Torsatron/Stellarator Laboratory, Univ. of Wisconsin-Madison) (1993).

[14] SHAING, K. C., et al., Phys. Fluids **B1**(1989)148.

[15] MAASSBERG, H., et al., Phys. Fluids **B5**(1993)3728.

[16] NÜHRENBERG, J., in Theory of Fusion Plasmas (Proc. Workshop Varenna, 1994) Editrice Compositori, Bologna (1994)3.

[17] GARABEDIAN, P., Phys. Plasmas **3**(1996)2483.

[18] NAKAJIMA, N., YOKOYAMA, M., OKAMOTO, M., NÜHRENBERG, J., Plasma Phys. Reports **23**(1997)460.

[19] HIRSHMAN. S. P., et al.. Comput. Phys. Commun. **43**(1986)143.

[20] FREIDBERG, J. P., Ideal Magnetohydrodynamics (Plenum Press, New York, 1987).

[21] NAKAJIMA. N., Phys. Plasmas **3**(1996)4545.

[22] NAKAJIMA. N., Phys. Plasmas **3**(1996)4556.

[23] HIRSHMAN, S. P., WHISTON, J. C., Phys. Fluids **26**(1983)3553.

[24] NÜHRENBERG, C., Phys. Plasmas **3**(1996)2401.

[25] ICHIGUCHI, K., NAKAJIMA, N., OKAMOTO, M., Nucl. Fusion **37**(1997)1109.

[26] MERCIER, C., Nucl. Fusion **1**(1960)47.

[27] LOTZ, W., et al., Plasma Phys. Control. Fusion **34**(1992)1037.

[28] HAMBERGER, S. M., et al., Fusion Technol. **17**(1990)123.

[29] HAYASHI, T., SATO, T., et al., Phys. Plasmas **2**(1995)752.

	R_{11} m	Z_{11} m	$R_{1,-1}$ m	$Z_{1,-1}$ m	$\iota(0)/\iota(a)$	Well(%)	$B_{01}(0)/B_{01}(a)$ (%)
Conf. 1	−0.20	0.30	0.00	0.00	0.172/0.186	−2.61	0.33/ − 2.66
Conf. 2	−0.20	0.18	0.04	0.06	0.113/0.122	1.06	1.12/ − 2.24
Conf. 3	−0.20	0.18	0.08	0.00	0.103/0.113	0.59	0.62/ − 1.68

Table. I Several combinations of $R_{11}, Z_{11}, R_{1,-1}$ and $Z_{1.-1}$ satisfying eq. (6) and some MHD equilibrium quantities.

	E_{RZ}	R_{11}/R_{10}	Z_{11}/R_{10}	$R_{1,-1}/R_{10}$	$Z_{1,-1}/R_{10}$	Residue
low-ι	1.31	−0.36	0.36	−0.05	−0.05	−0.208
standard	1.31	−0.46	0.46	−0.025	−0.025	−0.173
high-ι	1.29	−0.55	0.55	0.0018	0.0018	−0.123

Table. II The ratios $R_{11}/R_{10}, Z_{11}/R_{10}, R_{1,-1}/R_{10}$ and $Z_{1,-1}/R_{10}$ for the three magnetic configurations in the W7-X [24]. The residue of eq. (6) is also listed.

	$\iota(0)/\iota(a)$	Well (%)	B_{mn}s (%)		
QA1	0.094/0.118	0.61	(B_{21})8.91	(B_{01})6.46/1.15	(B_{11})5.32
QA2	0.108/0.144	−21.0	(B_{01})4.79/4.62	(B_{31}) − 3.35	(B_{12}) − 3.26
QA3	0.100/0.130	−13.7	(B_{01})5.40/4.94	(B_{21})5.09	(B_{12}) − 3.59
QA4	0.126/0.129	−6.44	(B_{21})3.80	(B_{12}) − 2.65	(B_{02})0.43/2.18
QA5	0.113/0.137	0.41	(B_{02})1.82/4.90	(B_{12}) − 4.21	(B_{01})1.20/3.30
QA6	0.118/0.139	0.41	(B_{01})0.47/4.03	(B_{02})1.04/3.63	(B_{21}) − 3.07
QA7	0.119/0.136	1.15	(B_{01}) − 0.33/3.72	(B_{22}) − 3.09/3.63	(B_{21})2.30

Table. III Several MHD equilibrium quantities for the magnetic configurations to approach a QAS configuration.

	$\iota(0)/\iota(a)$	Well (%)	$B_{10}/(a/R_{maj})$	B_{mn}s (%)			
QH1	0.195/0.208	−2.67	1.01	$(B_{10})-8.06$	$(B_{01})4.12/3.32$	$(B_{11})3.73$	$(B_{21})2.11$
QH2	0.238/0.247	−4.45	0.18	$(B_{11})-7.81$	$(B_{01})2.47/1.86$	$(B_{21})2.46$	$(B_{12})1.48$
QH3	0.244/0.265	0.27	0.12	$(B_{11})-10.7$	$(B_{01})1.05/2.45$	$(B_{12})1.79$	$(B_{1,-1})1.05$
QH4	0.244/0.267	2.44	0.12	$(B_{11})-10.4$	$(B_{12})1.46$	$(B_{1,-1})1.43$	$(B_{21})-1.34$

Table. IV Several MHD equilibrium quantities for the magnetic configurations to approach a QHS configuration.

M	$R_{01}/R_{10}=-Z_{01}/R_{10}$
3	2.24
4	1.18
5	0.66
6	0.41

Table. V The ratios, $R_{01}/R_{10}=-Z_{01}/R_{10}$, used to reduce B_{10} in different field period numbers.

Figure Captions

Fig. 1: Magnetic surface cross sections of the basic configuration.

Fig. 2: **(a)** Magnetic surface cross sections of four axisymmetric configurations with different geometrical aspect ratio.

(b) The normalized magnetic field strength on the equatorial plane for four configurations shown in Fig. 2(a) with corresponding colors.

Fig. 3: **(a)** Magnetic surface cross sections of the configurations with elliptic shape for $M = 2$ (Fig. 3.1), $M = 5$ (Fig. 3.2) and $M = 10$ (Fig. 3.3). The cross section at $\phi = 0$ $((1/4)(2\pi/M), (1/2)(2\pi/M))$ is colored green (blue, red), respectively.

(b) The magnetic field spectra in the Boozer coordinates for the configurations shown in Figs. 3.1(a), 3.2(a) and 3.3(a).

Fig. 4: Rotational transform profile per period for $M = 2, 5$ and 10 cases shown in Figs. 3.

Fig. 5: **(a)** Magnetic surface cross sections of the configuration with $R_{11}/R_{10} = -0.5$ on the basic configuration. The cross section at $\phi = 0$ $((1/4)(2\pi/M)$, $(1/2)(2\pi/M))$ is colored green (blue, red), respectively.

(b) The local rotational transform $\hat{\iota}$ on the outermost magnetic surface for the configuration shown in Fig. 5(a).

Fig. 6: **(a)** Magnetic surface cross sections of the configuration with $Z_{11}/R_{10} = 0.75$ on the basic configuration. The cross section at $\phi = 0$ $((1/4)(2\pi/M)$, $(1/2)(2\pi/M))$ is colored green (blue, red), respectively.

(b) The local rotational transform $\hat{\iota}$ on the outermost magnetic surface for the configuration shown in Fig. 6(a).

Fig. 7: **(a)** The magnetic field spectra in the Boozer coordinates for the configuration shown in Fig. 5(a).

(b) The magnetic field spectra in the Boozer coordinates for the configuration shown in Fig. 6(a).

Fig. 8: **(a)** Magnetic surface cross sections of the configuration with $(R_{11}/R_{10}, Z_{11}/R_{10}) = (-0.5, 0.75)$ on the basic configuration. The cross section at $\phi = 0$ $((1/4)(2\pi/M), (1/2)(2\pi/M))$ is colored green (blue, red), respectively.

(b) The magnetic field spectra in the Boozer coordinates for the configuration shown in Fig. 8(a).

Fig. 9: **(a)** The rotational transform at the magnetic axis, $\iota(0)$, as a function of (R_{11}, Z_{11}).

(b) The magnetic well depth (negative value for magnetic hill) (%) as a function of (R_{11}, Z_{11}).

(c) The bumpy field component at the magnetic axis, $B_{01}(0)$, as a function of (R_{11}, Z_{11}).

Fig. 10: **(a)** Magnetic surface cross sections of the configuration "Conf. 2" listed in Table I. The cross section at $\phi = 0$ $((1/4)(2\pi/M), (1/2)(2\pi/M))$ is colored green (blue, red), respectively.

(b) Magnetic surface cross sections of the configuration "Conf. 3" listed in Table I. The cross section at $\phi = 0$ $((1/4)(2\pi/M), (1/2)(2\pi/M))$ is colored green (blue, red), respectively.

Fig. 11: **(a)** Magnetic surface cross sections of the configuration with $R_{21}/R_{10} = 0.25$ on the basic configuration. The cross section at $\phi = 0$ $((1/4)(2\pi/M)$, $(1/2)(2\pi/M))$ is colored green (blue, red), respectively.

(b) The local rotational transform $\hat{\iota}$ at $r/a = 0.3, 0.6$ and 1.0 (from top to bottom) for the configuration shown in Fig. 11(a).

(c) The magnetic field spectra in the Boozer coordinates for the configuration shown in Fig. 11(a).

Fig. 12: Magnetic surface cross sections of the configuration with $(R_{21}/R_{10}, Z_{21}/R_{10}) = (0.25, 0.25)$ on the "Conf. 1". The cross section at $\phi = 0$ $((1/4)(2\pi/M)$, $(1/2)(2\pi/M))$ is colored green (blue, red), respectively.

Fig. 13: **(a)** Magnetic surface cross sections of the configuration with $R_{01}/R_{10} = 0.5$ on the basic configuration. The cross section at $\phi = 0$ $((1/4)(2\pi/M)$, $(1/2)(2\pi/M))$ is colored green (blue, red), respectively.

(b) The magnetic field spectra in the Boozer coordinates for the configuration shown in Fig. 13(a).

Fig. 14: **(a)** Magnetic surface cross sections of the configuration with $Z_{01}/R_{10} = -0.5$ on the basic configuration. The cross section at $\phi = 0$ $((1/4)(2\pi/M)$, $(1/2)(2\pi/M))$ is colored green (blue, red), respectively.

(b) The magnetic field spectra in the Boozer coordinates for the configuration shown in Fig. 14(a).

Fig. 15: Magnetic surface cross sections of the configuration with $(R_{01}/R_{10}, Z_{01}/R_{10}) = (0.5, -0.25)$ on the "Conf. 4". The cross section at $\phi = 0$ $((1/4)(2\pi/M)$, $(1/2)(2\pi/M))$ is colored green (blue, red), respectively.

Fig. 16: The local rotational transform $\hat{\iota}$ at $r/a = 0.3, 0.6$ and 1.0 (from top to bottom) for the configuration with $R_{22}/R_{10} = 0.125$ on the basic configuration.

Fig. 17: Magnetic surface cross sections for **(a)** QA1, **(b)** QA3, **(c)** QA4, **(d)** QA5 and **(e)** QA7. The cross section at $\phi = 0((1/4)(2\pi/M), (1/2)(2\pi/M))$ is colored green (blue, red), respectively.

(f) The magnetic field spectra in the Boozer coordinates for the QA7.

Fig. 18: Magnetic surface cross sections for **(a)** QH1, **(b)** QH2, **(c)** QH3 and **(d)** QH4. The cross section at $\phi = 0$ $((1/4)(2\pi/M), (1/2)(2\pi/M))$ is colored green (blue, red), respectively.

(e) The magnetic field spectra in the Boozer coordinates for the QH4.

(f) Magnetic surface cross sections for a QHS configuration with $M = 5$. The cross section at $\phi = 0$ $((1/4)(2\pi/M), (1/2)(2\pi/M))$ is colored green (blue, red), respectively.

(g) The magnetic field spectra in the Boozer coordinates for the configuration shown in Fig. 18(f).

Fig. 19: **(a)** Magnetic surface cross sections obtained by changing R_{11}/R_{10} from -0.1 to 0 starting from the QH4. The cross section at $\phi = 0$ $((1/4)(2\pi/M)$, $(1/2)(2\pi/M))$ is colored green (blue, red), respectively.

(b) Magnetic surface cross sections for a QBS configuration with $M = 4$. The cross section at $\phi = 0$ $((1/4)(2\pi/M), (1/2)(2\pi/M))$ is colored green (blue, red), respectively.

(c) The magnetic field spectra in the Boozer coordinates for the configuration shown in Fig. 19(b).

Fig. 20: The classification of QAS, QHS and QBS configurations are shown based on the bumpy field control by considering eq. (6), field period number (M), geometrical aspect ratio (A_p) and magnetic axis excursion.

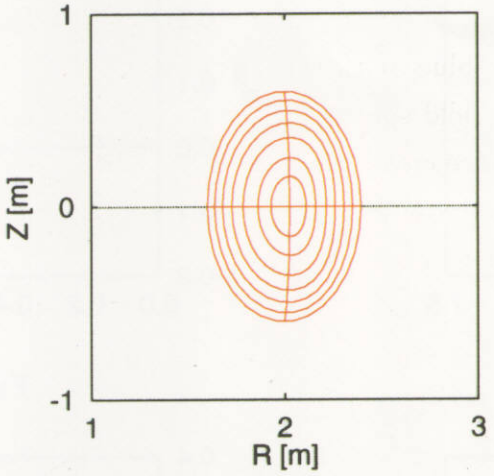

Fig. 1

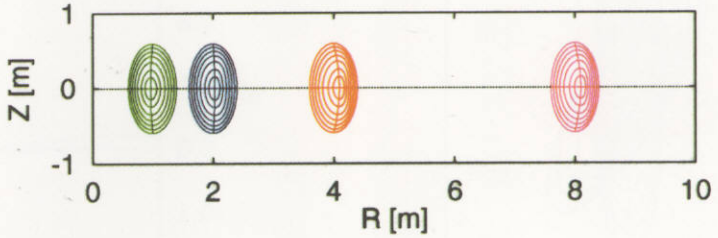

Fig. 2(a)

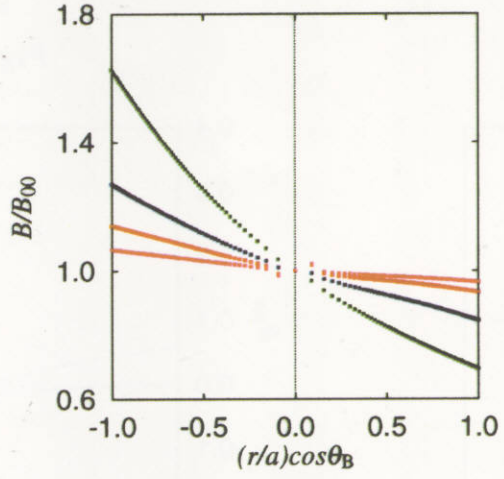

Fig. 2(b)

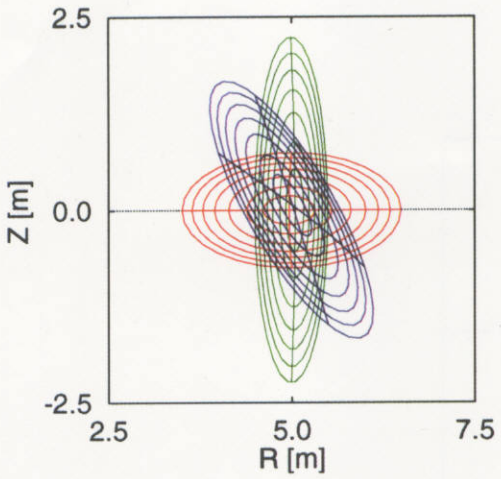

Fig. 3.1(a)

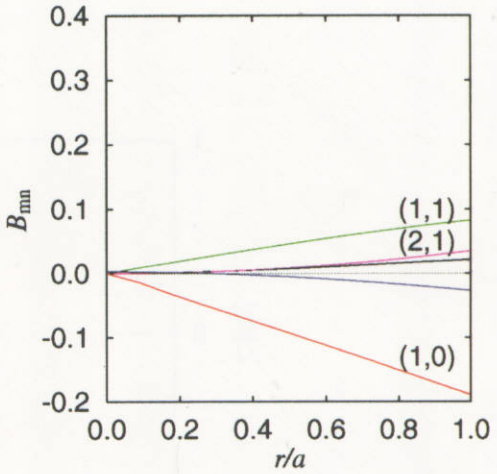

Fig. 3.1(b)

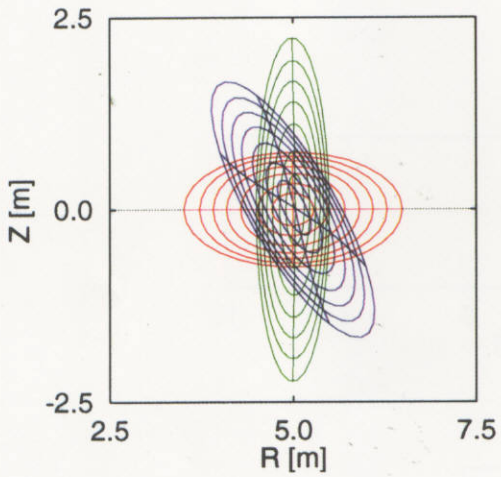

Fig. 3.2(a)

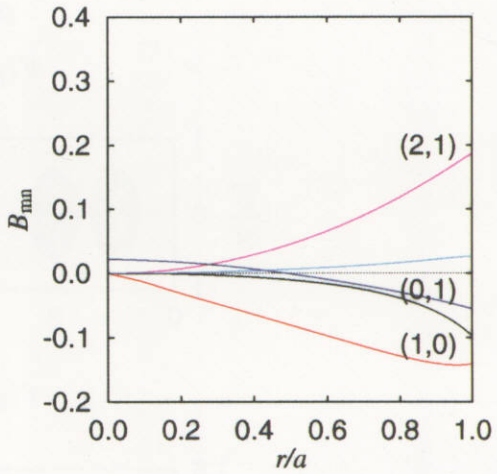

Fig. 3.2(b)

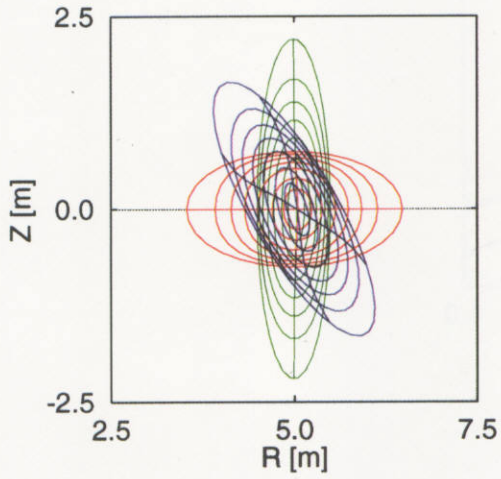

Fig. 3.3(a)

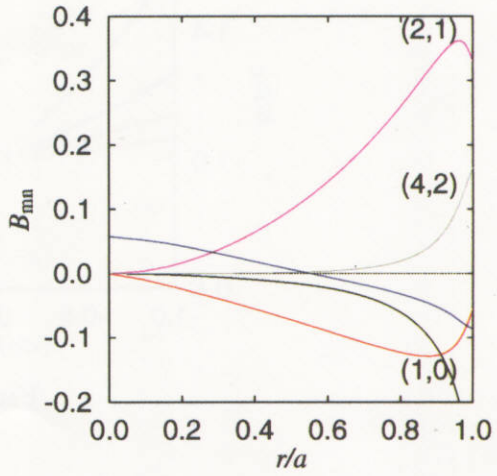

Fig. 3.3(b)

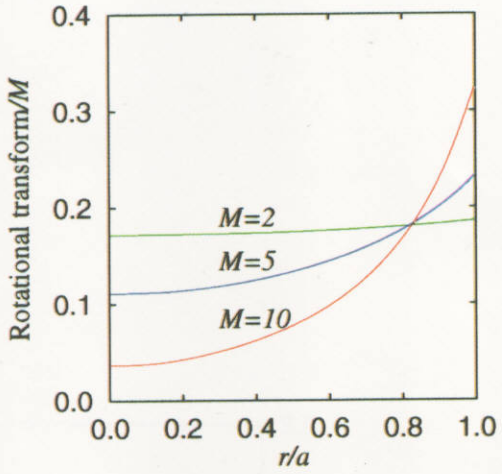

Fig. 4

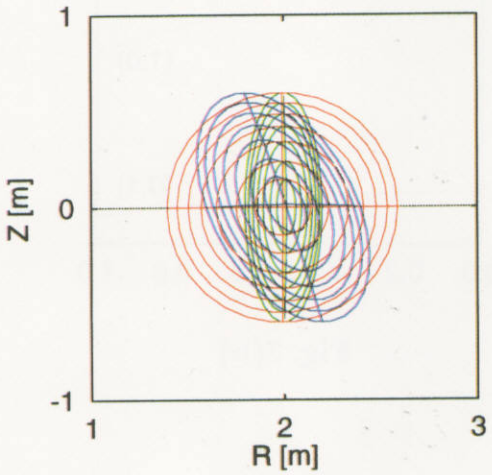

Fig. 5(a)

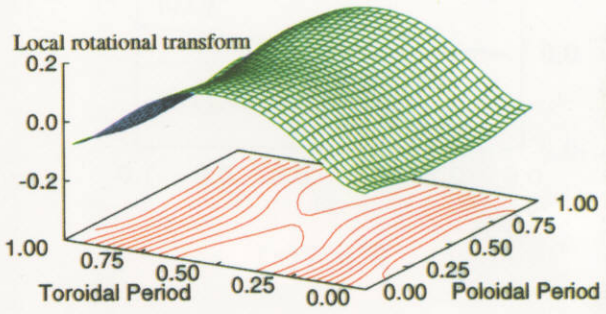

Fig. 5(b)

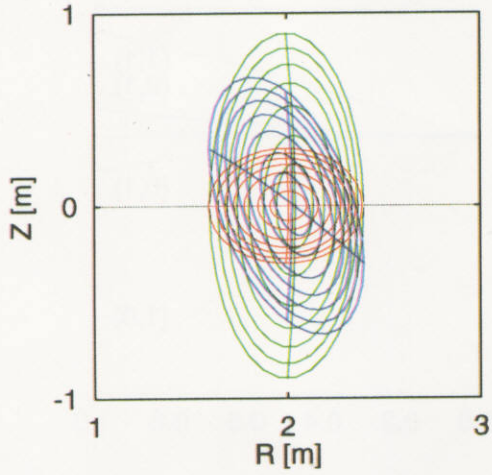

Fig. 6(a)

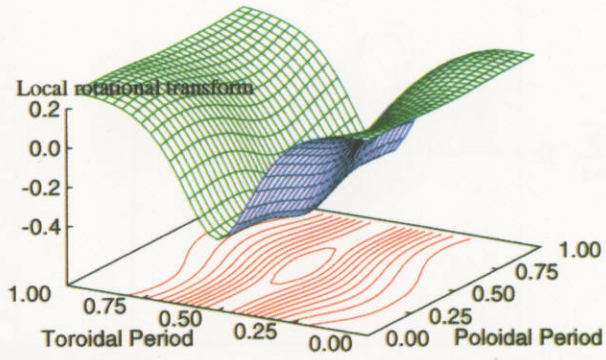

Fig. 6(b)

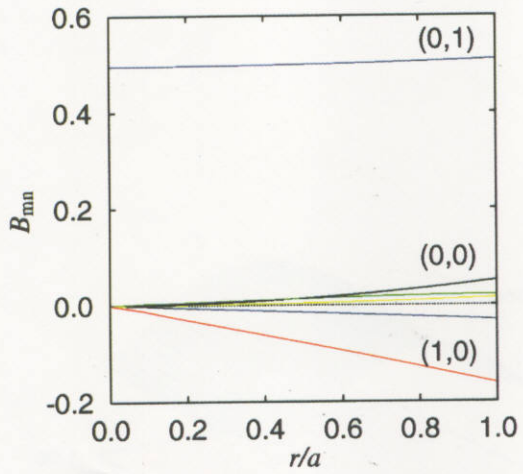

Fig. 7(a)

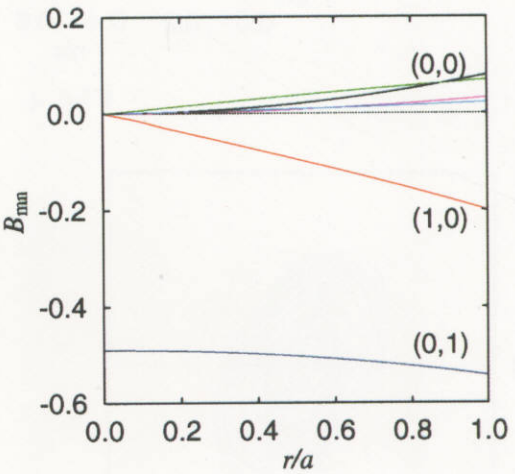

Fig. 7(b)

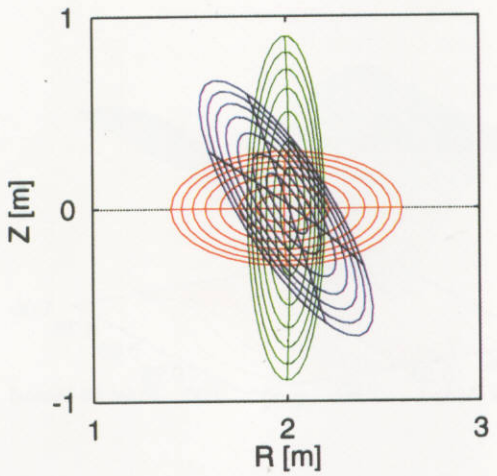

Fig. 8(a)

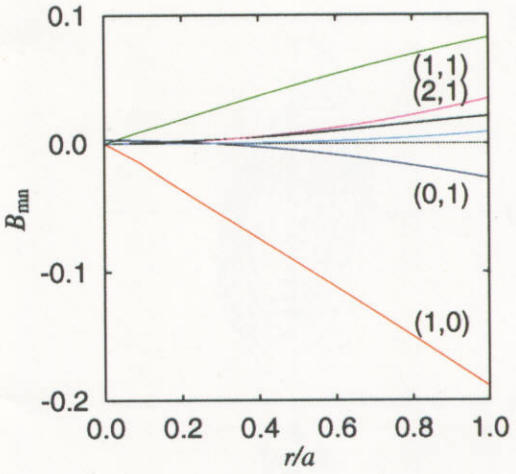

Fig. 8(b)

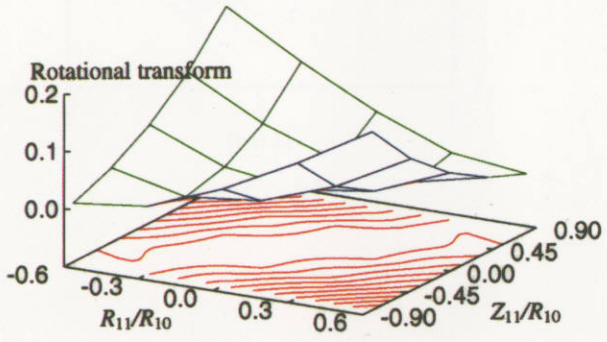

Fig. 9(a)

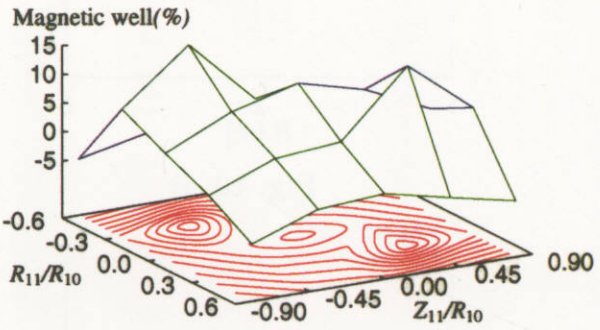

Fig. 9(b)

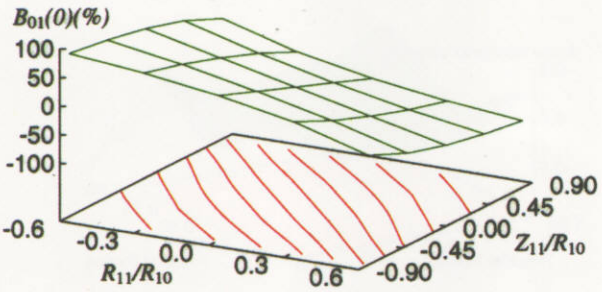

Fig. 9(c)

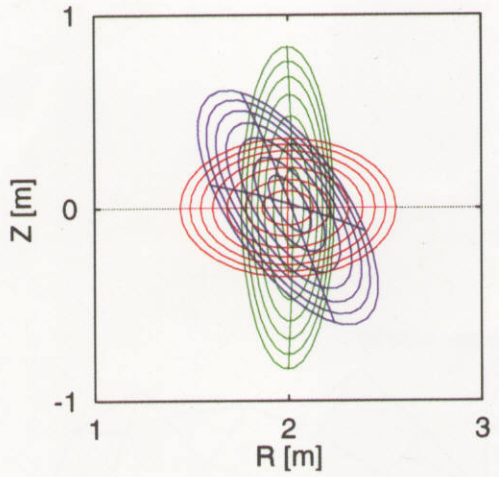

Fig. 10(a)

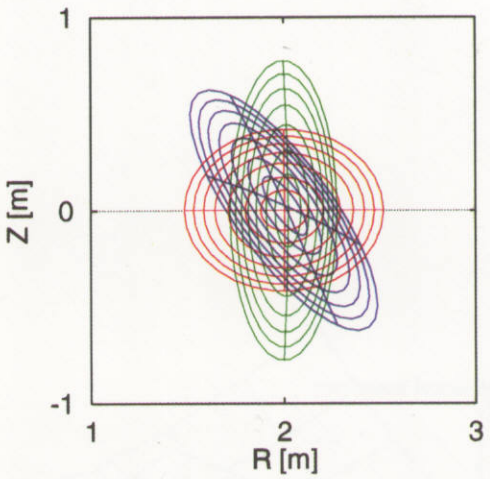

Fig. 10(b)

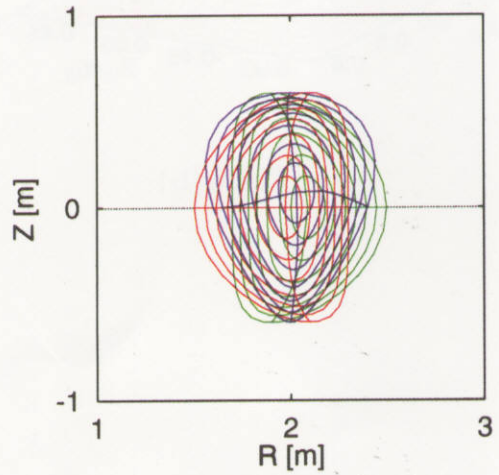

Fig. 11(a)

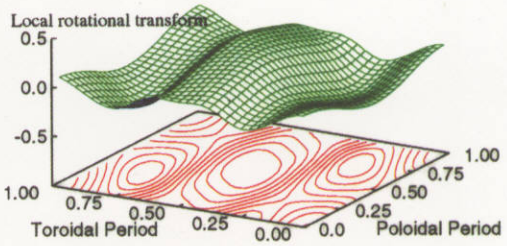

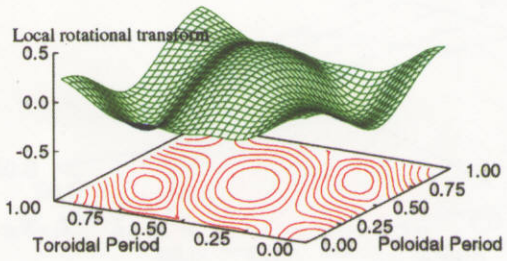

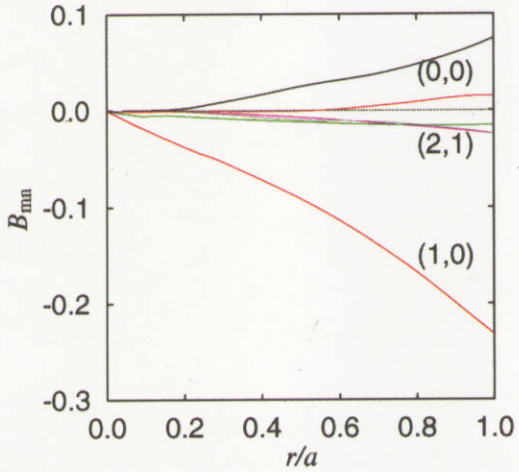

Fig. 11(c)

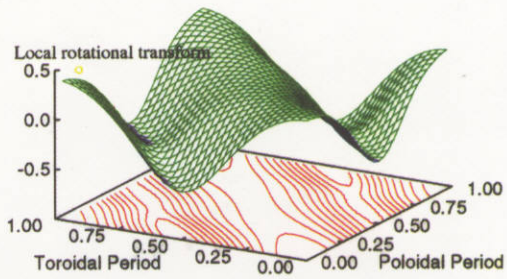

Fig. 11(b)

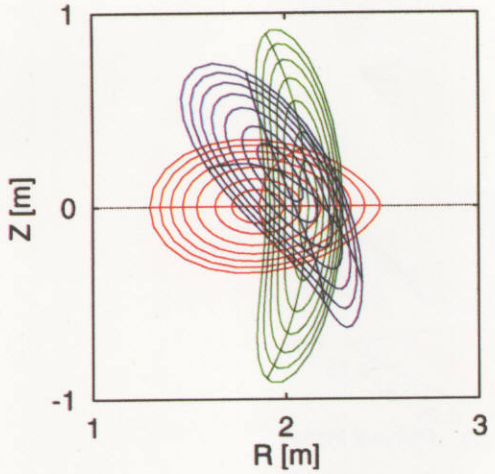

Fig. 12

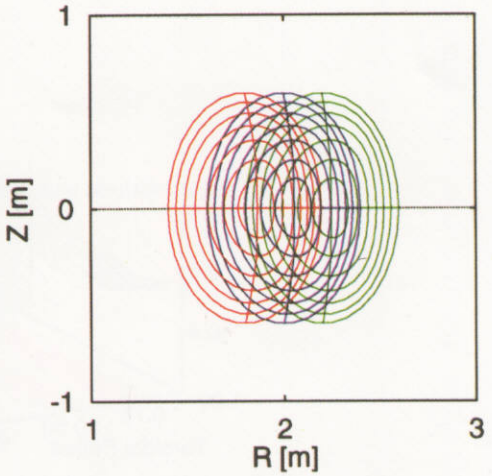

Fig. 13(a)

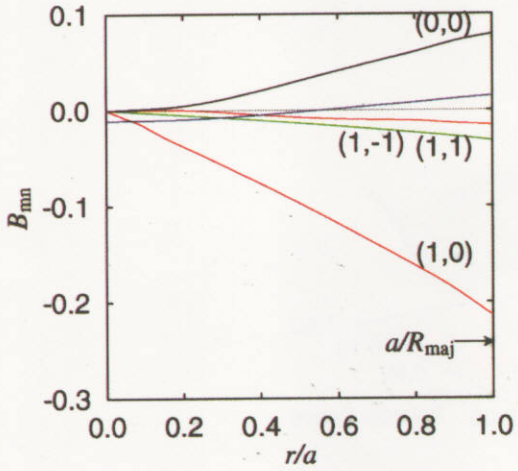

Fig. 13(b)

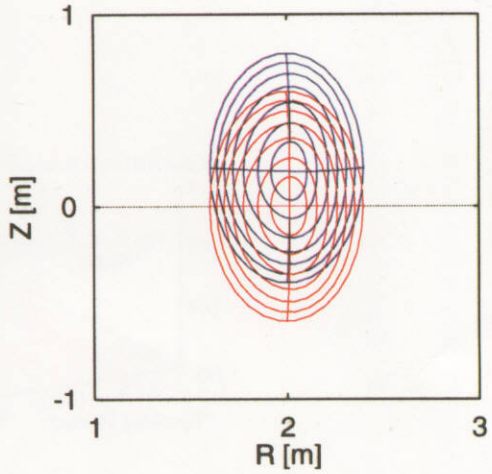

Fig. 14(a)

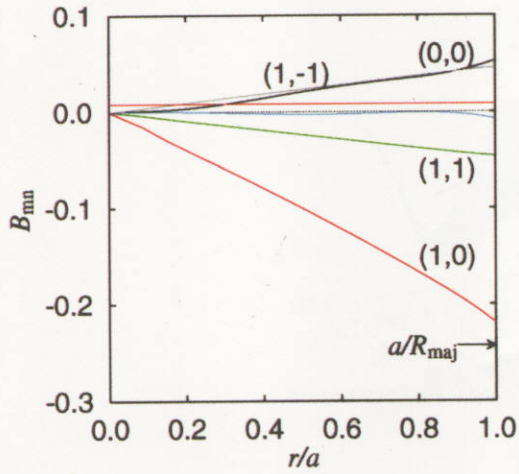

Fig. 14(b)

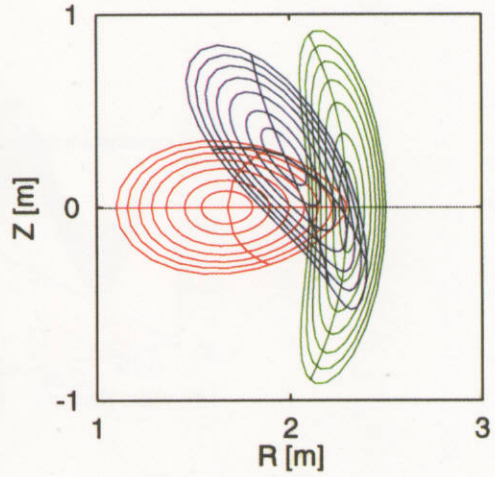

Fig. 15

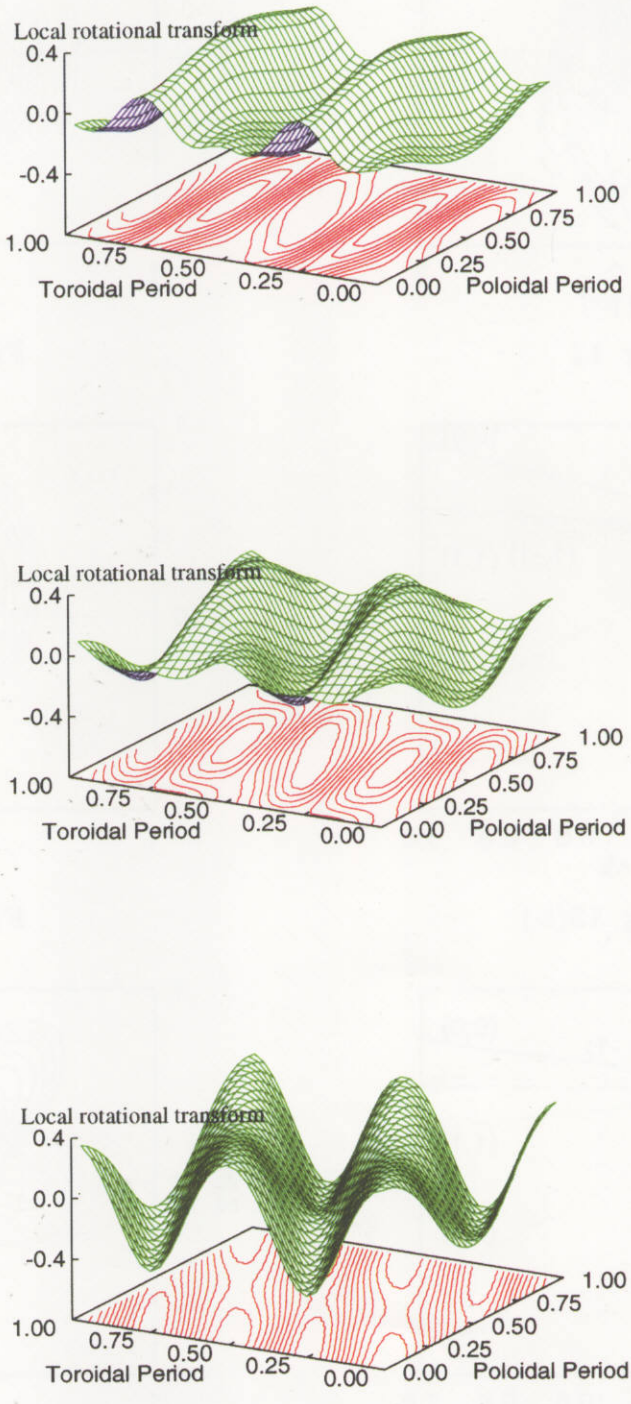
Local rotational transform
0.4
0.0
-0.4
1.00
0.75
0.50
0.25
0.00
Toroidal Period
0.00
0.25
0.50
0.75
1.00
Poloidal Period

Fig. 16

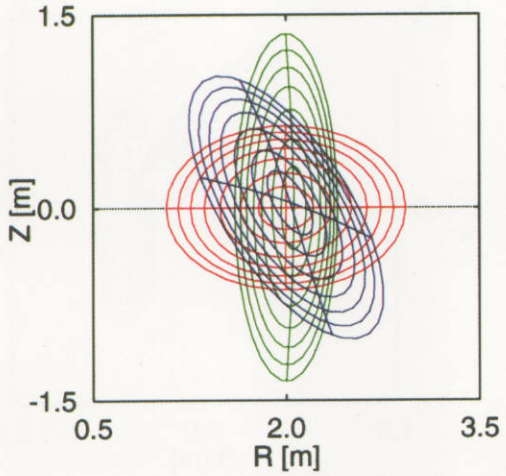

Fig. 17(a)

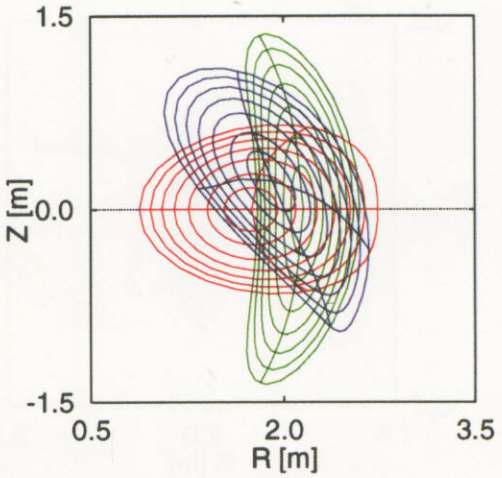

Fig. 17(b)

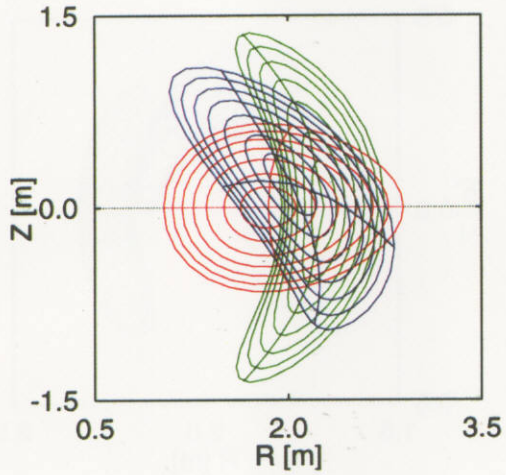

Fig. 17(c)

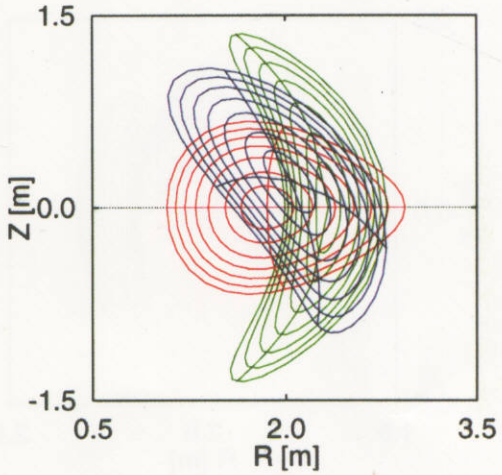

Fig. 17(d)

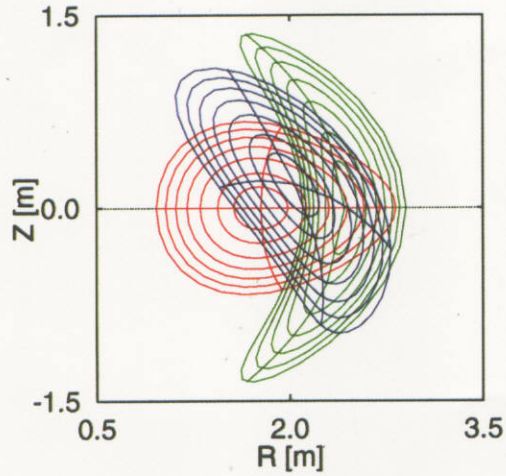

Fig. 17(e)

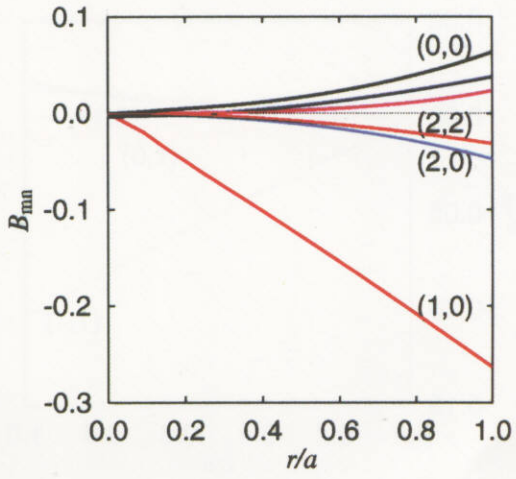

Fig. 17(f)

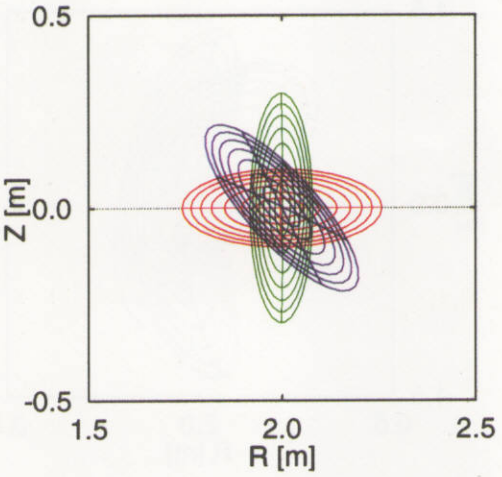

Fig. 18(a)

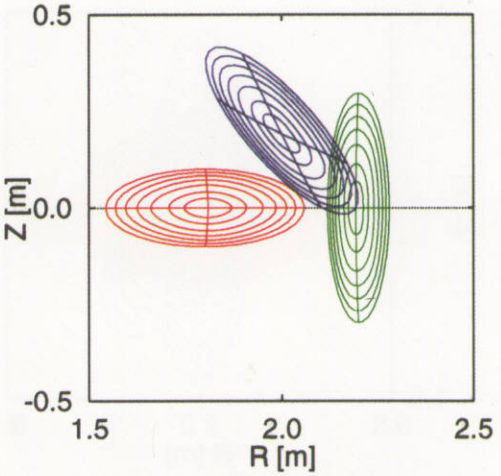

Fig. 18(b)

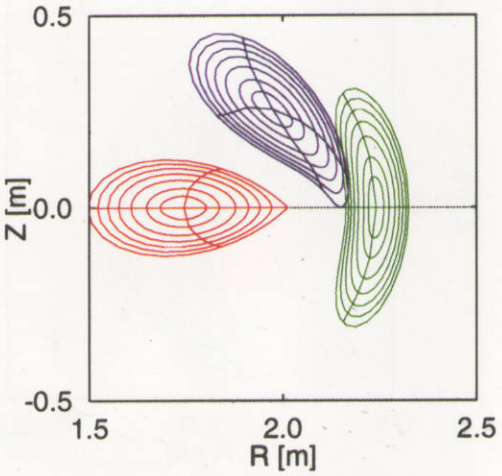

Fig. 18(c)

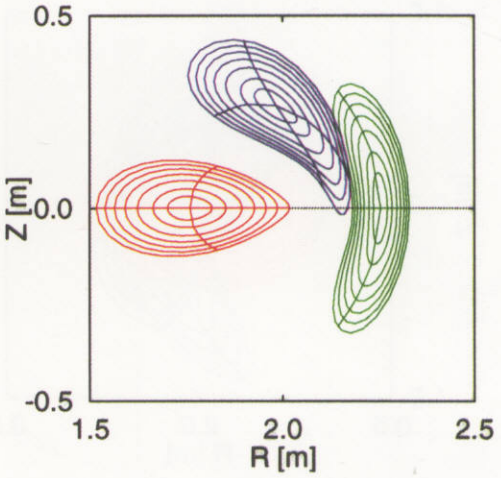

Fig. 18(d)

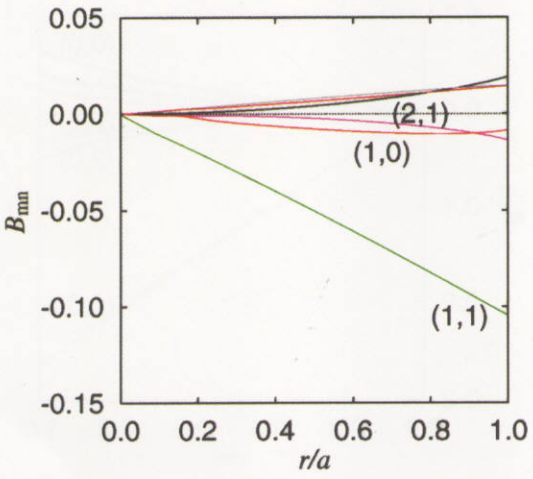

Fig. 18(e)

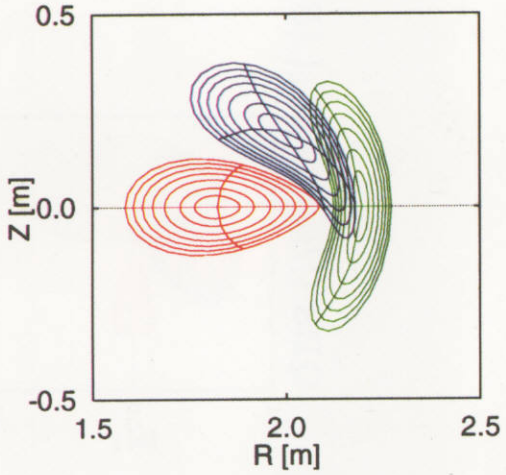

Fig. 18(f)

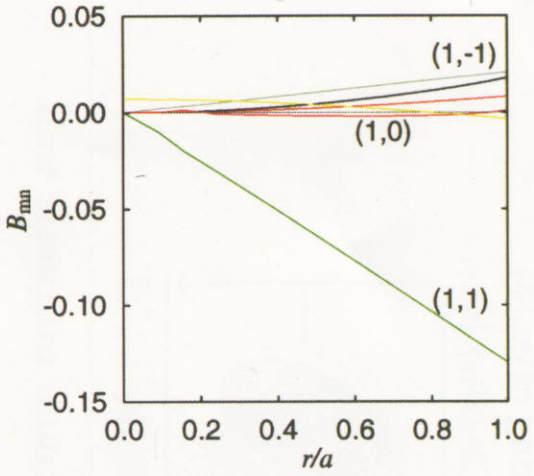

Fig. 18(g)

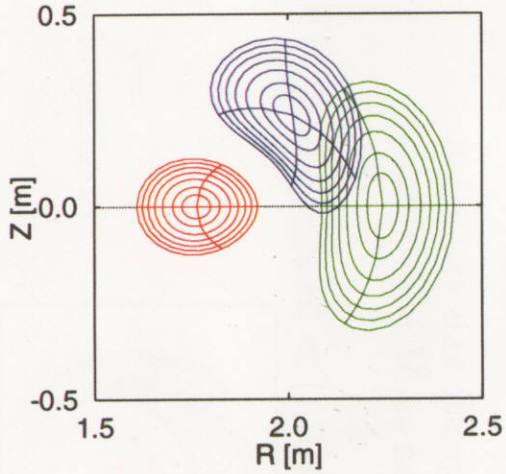

Fig. 19(a)

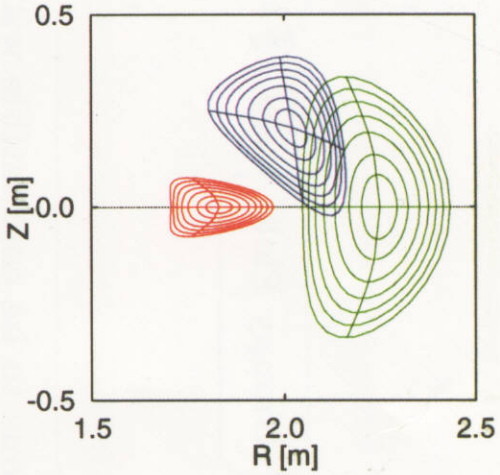

Fig. 19(b)

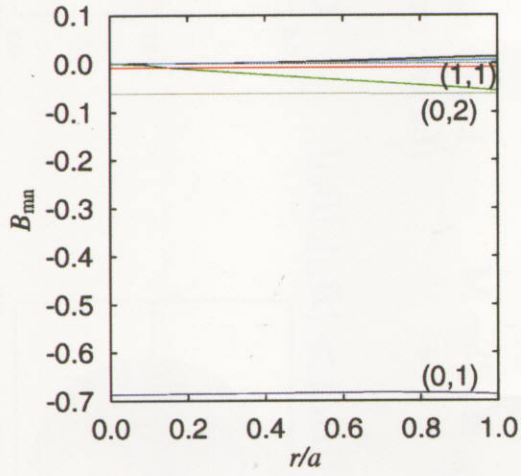

Fig. 19(c)

Fig. 20

satisfaction of eq.(5)
$|B_{01}| \ll |B_{10}|, |B_{11}|$

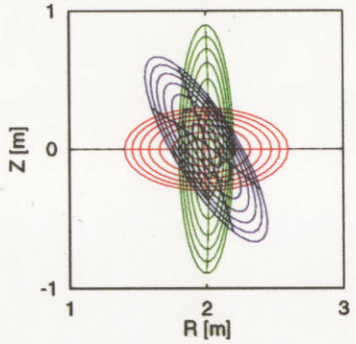

$\Longleftarrow$ **Bumpy Field** $\Longrightarrow$

breaking of eq.(5)
$|B_{01}| \gg |B_{10}|, |B_{11}|$

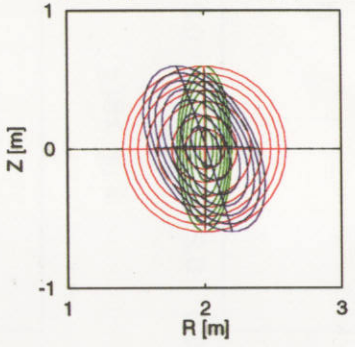

Typical magnetic surface cross sections to be compatible with vacuum magnetic well

$\phi \sim 0$: bean shape, $\phi \sim (1/4)(2\pi/M)$: tear-drop shape, $\phi \sim (1/2)(2\pi/M)$: outward pointing triangular shape

$\Longleftarrow$ **appropriate combinations of helical and triangular boundary modulations**

smaller A_p, smaller M

$\Downarrow$

QAS ($|B_{10}| \gg |B_{11}|, |B_{01}|$)

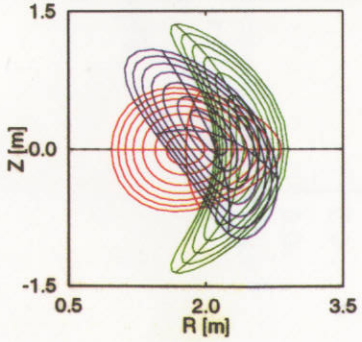

larger A_p, magnetic axis excursion
(larger excursion as M is decreased)

$\Downarrow$

QHS ($|B_{11}| \gg |B_{10}|, |B_{01}|$)

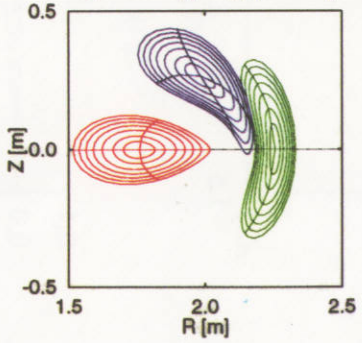

$\Longrightarrow$
breaking of eq.(5)

QBS ($|B_{01}| \gg |B_{10}|, |B_{11}|$)

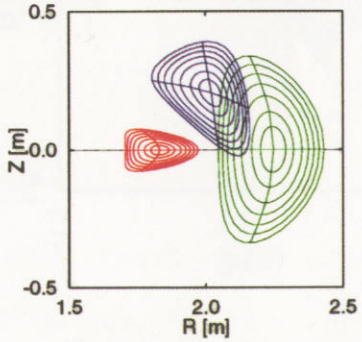

Recent Issues of NIFS Series

NIFS-474 K. Ohkubo, S. Kubo, H. Idei, M. Sato, T. Shimozuma and Y. Takita,
Coupling of Tilting Gaussian Beam with Hybrid Mode in the Corrugated Waveguide; Jan. 1997

NIFS-475 A. Fujisawa, H. Iguchi, S. Lee and Y. Hamada,
Consideration of Fluctuation in Secondary Beam Intensity of Heavy Ion Beam Prove Measurements; Jan. 1997

NIFS-476 Y. Takeiri, M. Osakabe, Y. Oka, K. Tsumori, O. Kaneko, T. Takanashi, E. Asano, T. Kawamoto, R. Akiyama and T. Kuroda,
Long-pulse Operation of a Cesium-Seeded High-Current Large Negative Ion Source; Jan. 1997

NIFS-477 H. Kuramoto, K. Toi, N. Haraki, K. Sato, J. Xu, A. Ejiri, K. Narihara, T. Seki, S. Ohdachi, K. Adati, R. Akiyama, Y. Hamada, S. Hirokura, K. Kawahata and M. Kojima,
Study of Toroidal Current Penetration during Current Ramp in JIPP T-IIU with Fast Response Zeeman Polarimeter; Jan., 1997

NIFS-478 H. Sugama and W. Horton,
Neoclassical Electron and Ion Transport in Toroidally Rotating Plasmas; Jan. 1997

NIFS-479 V.L. Vdovin and I.V. Kamenskij,
3D Electromagnetic Theory of ICRF Multi Port Multi Loop Antenna; Jan. 1997

NIFS-480 W.X. Wang, M. Okamoto, N. Nakajima, S Murakami and N. Ohyabu,
Cooling Effect of Secondary Electrons in the High Temperature Divertor Operation; Feb. 1997

NIFS-481 K. Itoh, S.-I. Itoh, H. Soltwisch and H.R. Koslowski,
Generation of Toroidal Current Sheet at Sawtooth Crash; Feb. 1997

NIFS-482 K. Ichiguchi,
Collisionality Dependence of Mercier Stability in LHD Equilibria with Bootstrap Currents; Feb. 1997

NIFS-483 S. Fujiwara and T. Sato,
Molecular Dynamics Simulations of Structural Formation of a Single Polymer Chain: Bond-orientational Order and Conformational Defects; Feb. 1997

NIFS-484 T. Ohkawa,
Reduction of Turbulence by Sheared Toroidal Flow on a Flux Surface; Feb. 1997

NIFS-485 K. Narihara, K. Toi, Y. Hamada, K. Yamauchi, K. Adachi, I. Yamada, K. N. Sato, K.

Kawahata, A. Nishizawa, S. Ohdachi, K. Sato, T. Seki, T. Watari, J. Xu, A. Ejiri, S. Hirokura, K. Ida, Y. Kawasumi, M. Kojima, H. Sakakita, T. Ido, K. Kitachi, J. Koog and H. Kuramoto,
Observation of Dusts by Laser Scattering Method in theJIPPT-IIU Tokamak Mar. 1997

NIFS-486 S. Bazdenkov, T. Sato and The Complexity Simulation Group,
Topological Transformations in Isolated Straight Magnetic Flux Tube; Mar. 1997

NIFS-487 M. Okamoto,
Configuration Studies of LHD Plasmas; Mar. 1997

NIFS-488 A. Fujisawa, H. Iguchi, H. Sanuki, K. Itoh, S. Lee, Y. Hamada, S. Kubo, H. Idei, R. Akiyama, K. Tanaka, T. Minami, K. Ida, S. Nishimura, S. Morita, M. Kojima, S. Hidekuma, S.-I. Itoh, C. Takahashi, N. Inoue, H. Suzuki, S. Okamura and K. Matsuoka,
Dynamic Behavior of Potential in the Plasma Core of the CHS Heliotron/Torsatron; Apr. 1997

NIFS-489 T. Ohkawa,
Pfirsch - Schlüter Diffusion with Anisotropic and Nonuniform Superthermal Ion Pressure; Apr. 1997

NIFS-490 S. Ishiguro and The Complexity Simulation Group,
Formation of Wave-front Pattern Accompanied by Current-driven Electrostatic Ion-cyclotron Instabilities; Apr. 1997

NIFS-491 A. Ejiri, K. Shinohara and K. Kawahata,
An Algorithm to Remove Fringe Jumps and its Application to Microwave Reflectometry; Apr. 1997

NIFS-492 K. Ichiguchi, N. Nakajima, M. Okamoto,
Bootstrap Current in the Large Helical Device with Unbalanced Helical Coil Currents; Apr. 1997

NIFS-493 S. Ishiguro, T. Sato, H. Takamaru and The Complexity Simulation Group,
V-shaped dc Potential Structure Caused by Current-driven Electrostatic Ion-cyclotron Instability; May 1997

NIFS-494 K. Nishimura, R. Horiuchi, T. Sato,
Tilt Stabilization by Energetic Ions Crossing Magnetic Separatrix in Field-Reversed Configuration; June 1997

NIFS-495 T. -H. Watanabe and T. Sato,
Magnetohydrodynamic Approach to the Feedback Instability; July 1997

NIFS-496 K. Itoh, T. Ohkawa, S. -I.Itoh, M. Yagi and A. Fukuyama
Suppression of Plasma Turbulence by Asymmetric Superthermal Ions; July 1997

NIFS-497 T. Takahashi, Y. Tomita, H. Momota and Nikita V. Shabrov,
Collisionless Pitch Angle Scattering of Plasma Ions at the Edge Region of an FRC; July 1997

NIFS-498 M. Tanaka, A.Yu Grosberg, V.S. Pande and T. Tanaka,
Molecular Dynamics and Structure Organization in Strongly-Coupled Chain of Charged Particles; July 1997

NIFS-499 S. Goto and S. Kida,
Direct-interaction Approximation and Reynolds-number Reversed Expansion for a Dynamical System; July 1997

NIFS-500 K. Tsuzuki, N. Inoue, A. Sagara, N. Noda, O. Motojima, T. Mochizuki, T. Hino and T. Yamashina,
Dynamic Behavior of Hydrogen Atoms with a Boronized Wall; July 1997

NIFS-501 I. Viniar and S. Sudo,
Multibarrel Repetitive Injector with a Porous Pellet Formation Unit; July 1997

NIFS-502 V. Vdovin, T. Watari and A. Fukuyama,
An Option of ICRF Ion Heating Scenario in Large Helical Device; July 1997

NIFS-503 E. Segre and S. Kida,
Late States of Incompressible 2D Decaying Vorticity Fields; Aug. 1997

NIFS-504 S. Fujiwara and T. Sato,
Molecular Dynamics Simulation of Structural Formation of Short Polymer Chains; Aug. 1997

NIFS-505 S. Bazdenkov and T. Sato
Low-Dimensional Model of Resistive Interchange Convection in Magnetized Plasmas; Sep. 1997

NIFS-506 H. Kitauchi and S. Kida,
Intensification of Magnetic Field by Concentrate-and-Stretch of Magnetic Flux Lines; Sep. 1997

NIFS-507 R.L. Dewar,
Reduced form of MHD Lagrangian for Ballooning Modes; Sep. 1997

NIFS-508 Y.-N. Nejoh,
Dynamics of the Dust Charging on Electrostatic Waves in a Dusty Plasma with Trapped Electrons; Sep.1997

NIFS-509 E. Matsunaga, T.Yabe and M. Tajima,
Baroclinic Vortex Generation by a Comet Shoemaker-Levy 9 Impact; Sep. 1997

NIFS-510 C.C. Hegna and N. Nakajima,
On the Stability of Mercier and Ballooning Modes in Stellarator Configurations; Oct. 1997

NIFS-511 K. Orito and T. Hatori,
Rotation and Oscillation of Nonlinear Dipole Vortex in the Drift-Unstable Plasma; Oct. 1997

NIFS-512 J. Uramoto,
Clear Detection of Negative Pionlike Particles from H_2 Gas Discharge in Magnetic Field; Oct. 1997

NIFS-513 T. Shimozuma, M. Sato, Y. Takita, S. Ito, S. Kubo, H. Idei, K. Ohkubo, T. Watari, T.S. Chu, K. Felch, P. Cahalan and C.M. Loring, Jr,
The First Preliminary Experiments on an 84 GHz Gyrotron with a Single-Stage Depressed Collector; Oct. 1997

NIFS-514 T. Shjmozuma, S. Morimoto, M. Sato, Y. Takita, S. Ito, S. Kubo, H. Idei, K. Ohkubo and T. Watari,
A Forced Gas-Cooled Single-Disk Window Using Silicon Nitride Composite for High Power CW Millimeter Waves; Oct. 1997

NIFS-515 K. Akaishi,
On the Solution of the Outgassing Equation for the Pump-down of an Unbaked Vacuum System; Oct. 1997

NIFS-516 *Papers Presented at the 6th H-mode Workshop (Seeon, Germany)*; Oct. 1997

NIFS-517 John L. Johnson,
The Quest for Fusion Energy; Oct. 1997

NIFS-518 J. Chen, N. Nakajima and M. Okamoto,
Shift-and-Inverse Lanczos Algorithm for Ideal MHD Stability Analysis; Nov. 1997

NIFS-519 M. Yokoyama, N. Nakajima and M. Okamoto,
Nonlinear Incompressible Poloidal Viscosity in L=2 Heliotron and Quasi-Symmetric Stellarators; Nov. 1997

NIFS-520 S. Kida and H. Miura,
Identificaiton and Analysis of Vortical Structures; Nov. 1997

NIFS-521 K. Ida, S. Nishimura, T. Minami, K. Tanaka, S. Okamura, M. Osakabe, H. Idei, S. Kubo, C. Takahashi and K. Matsuoka,
High Ion Temperature Mode in CHS Heliotron/torsatron Plasmas; Nov. 1997

NIFS-522 M. Yokoyama, N. Nakajima and M. Okamoto,
Realization and Classification of Symmetric Stellarator Configurations through Plasma Boundary Modulations; Dec. 1997